Water storage and potential hazard of moraine-dammed glacial lake in maritime glaciation region—A case study of Bienong Co

Hongyu Duan[1], Xiaojun Yao[1], Yuan Zhang[1], Huian Jin[2], Qi Wang[3], Zhishui Du[3], Jiayu Hu[1], Bin Wang[4], Qianxun Wang[5]

[1] College of Geography and Environment Science, Northwest Normal University, LanZhou, 730070, China
[2] Gansu Forestry Polytechnic, Tianshui, 741020, China
[3] Northwest Engineering Corporation Limited, Power China, Xi'an 710065, China
[4] Xinjiang Transport Planning Survey and Design Institute Company Limited, Urumqi 830006, China
[5] Capital Urban Planning and Design Consulting Development Company Limited, Beijing 100038, China

Correspondence to: Xiaojun Yao (xj_yao@nwnu.edu.cn)

Abstract. The existence of glacial lakes in the Southeastern Tibetan Plateau (SETP) is a potential hazard to downstream regions, as the failure of some lakes has the potential to result in disastrous glacial lake outburst flood (GLOF) events of high-magnitude. In the present study, we conducted a comprehensive investigation for Bienong Co, an end moraine-dammed glacial lake in SETP. First, the lake basin morphology was simulated and the water storage was estimated, obtaining that the maximum lake depth is ~181 m and the water storage of ~102.3×10^6 m^3. Then, we assumed the ice avalanche (Scenarios A1, A2 and A3) and lateral moraine landslide (Scenarios B1, B2, B3 and C1, C2, C3) induced GLOFs process chain of Bienong Co. The volume of nine scenarios of trigger was calculated using RAMMS model and the displacement wave generation and propagation in the lake, overtopping flow and erosion on moraine dam and subsequent downstream flooding were simulated by BASEMENT model. The results show that the ice avalanche scenarios produce the largest amount of material into the lake, resulting in displacement wave amplitudes of up to 25.2 m (Scenario A3) near the moraine dam. And smaller volume of landslide entering the lake only result in smaller displacement waves in the lake, such as Scenario C1 has wave amplitude below 1 m near the moraine dam. Scenarios A1, A2 and A3 result in the released water from the lake of 24.1×10^6 m^3, 25.3×10^6 m^3 and 26.4×10^6 m^3, and the peak discharges at moraine dam of 4,996 m^3/s, 7,817 m^3/s and 13,078 m^3/s, respectively. These high discharges cause scour erosion of the moraine dams, resulting in breaches widths of 295.0 m, 339.4 m, 368.5 m, and breach depths of 19.0 m, 19.1 m, 19.3 m, respectively. However, in landslide scenarios, only the overtopping flow generated by Scenarios B3 and C3 caused moderate erosion of the moraine dam, with breach depth of 6.5 m and 7.9 m, and breach width of 153 m and 169 m, respectively. GLOFs generated by Scenario A1, A2 and A3 can all flow through 18 settlements downstream, and will threaten more than half of the settlements. Both Scenarios B3 and C3 produced floods that flow through eight downstream settlements within 20 hours and had a relatively small impact on them. Comparisons show that Bienong Co is the relative deepest glacial lake known on the Tibetan Plateau, and this study could provide a new insight of the moraine-dammed glacial lakes in the SETP and a reference for GLOFs disaster prevention to the local government.

1 Introduction

Due to global warming, the accelerated retreat and thinning of glaciers has occurred in most regions compared to the last century (Zemp et al., 2019), resulting in a rapid increase in the number, area, and volume of glacial lakes worldwide (Shugar et al., 2020; Wang et al., 2020). Glacier meltwater can be confined and stored in certain depressions dammed by moraine, ice or bedrock (Vilímek et al., 2013). Once the dam is damaged, the water can be suddenly and catastrophically released to form Glacial Lake Outburst Floods (GLOFs), which may cause severe social and geomorphic impacts several dozens of kilometers and more downstream (Lliboutry, 1977; Richardson and Reynolds, 2000; Osti and Egashira, 2009; Carrivick and Tweed, 2016; Cook et al., 2018; Zheng et al., 2021). Moraine-dammed glacial lakes are of particular attention owing to their large volume

(Fujita et al., 2013; Veh et al., 2020), weak dam composition, and exposure to various triggers, such as the ice and/or rock avalanches and heavy precipitation and intense glacier melting (Emmer and Cochachin, 2013; Nie et al., 2018), the most common sources of GLOFs (Watanbe and Rothacher, 1996; Westoby et al., 2014). The Himalayas and Southeastern Tibetan Plateau (SETP) are regions of frequently occurrence of GLOFs caused by moraine-dammed glacial lakes (Wang, 2016). Study shows that the Himalayas, especially the southern region is likely to experience more GLOFs at the coming decades (Veh et al., 2020).

The SETP is a broad mountainous area covering the central and eastern Nyainqêntanglha Ranges, eastern Himalayas and western Hengduan Mountains and has the most complicated terrains (Ke et al., 2014). Controlling by the warm and humid Indian monsoon, a plenty of maritime glaciers have developed here (Yang et al., 2008), featured as the adequate recharge, strong ablation, low snowline distribution, high temperature, fast movement, and strong geological as well as geomorphological effect (Li et al., 1986; Qin et al., 2007; Liu et al., 2014), which have been observed with the most negative mass balances during the past decades (Kääb et al., 2012; Neckel et al., 2014; Kääb et al., 2015; Brun et al., 2017; Dehecq et al., 2019). Therefore, the combination of active glacial processes and heavy rainfall during the monsoon season makes the region prone to glacier-related natural hazards (Wang et al., 2012b). Studies of glacial lakes in the SETP mainly focused on regional-scale assessment of glacial lake changes (Wang et al., 2011a; Song et al., 2016; Wang et al., 2017; Zhang et al., 2020; Zhang et al., 2021), identification of potentially dangerous glacial lakes (Wang et al., 2011; Liu et al., 2019; Duan et al., 2020; Qi et al., 2020), site-specific analysis of formation mechanism, development trend, risk evolution and management measures of GLOFs (Cui et al., 2003; Cheng et al., 2008, 2009; Sun et al., 2014; Liu et al., 2021; Wang et al., 2021), exploration of geological features of a single glacial lake (Yuan et al., 2012; Liu et al., 2015; Huang et al., 2016). Fewer studies applied hydrodynamic models to simulate GLOFs in the SETP. Wang et al. (2011b) evaluated the applicability of ASTER GDEM (Global Digital Elevation Model) and SRTM DEM in the simulation of GLOF process based on HEC RAS hydrodynamic model (Brunner, 2002). Zheng et al. (2021) analyzed and reconstructed a GLOF process chain of Jinwu Co using the published empirical relationships and GIS-based r.avaflow simulation tool (Mergili et al., 2017; Pudasaini and Mergili, 2019; Mergili and Pudasaini, 2020).

As a key factor related to the peak discharge and outburst volume of a GLOF event (Evans, 1987; Huggel et al., 2002), lake storage capacity is difficult to directly obtain by means of satellite remote sensing approach. Currently, owing to the easy availability of area information from remote sensing images, the volume of glacial lakes is generally estimated using the developed empirical formulas connect glacial lake area and volume based on bathymetric data for a small number of glacial lakes (O'Connor et al., 2001; Huggel et al., 2002; Yao et al., 2014). However, the estimated volume maybe inaccurate because the unique geographical conditions of different glacial lakes (Cook and Quincey, 2015). The SETP region is an area with high incidence of GLOFs (Sun et al., 2014; Zheng et al., 2021), however, there are few publicly available bathymetric data of glacial lakes and related research works. Previous bathymetric works in the Tibetan Plateau were carried out mainly for those glacial lakes located in the Himalayas (LIGG/WECS/NEA, 1988; Geological survey of India, 1995; Yamada, 1998; Mool et al., 2001; Sakai, 2003; Yamada, 2004; ICIMOD, 2011; Sakai, 2012; Yao et al., 2012; Wang et al., 2015; Haritashya et al., 2018; Sharma et al., 2018; Li et al., 2021). This is unfavorable to fully understand the morphology and disaster prevention of glacial lakes in the SETP region. In recent years, the Unmanned Surface Vessel (USV) have developed rapidly (Liu et al., 2016), which have been widely used in scenarios such as bathymetric map creation, transportation, environmental monitoring, and moraine surveys (Larrazabal and Peñas, 2016; Yan et al., 2010; Specht et al., 2019a) owing to the favorable security on personnel safety and and the high flexibility in complex environments. Glacial lakes are mostly located at high altitudes and in harsh environments (Zhang et al., 2020), and USV makes the measurement of the underwater topography of glacial lakes safer, more convenient, and more accurate (Li et al., 2021).

In this study, we aim to complete an investigation of the potential GLOF hazard of an end moraine-dammed glacial lake, Bienong Co (Co means lake in Tibetan) in the SETP based on field bathymetric data and remote sensing data using a multi-

model combination method. First, the lake basin morphology of Bienong Co is modelled. Then, multiple components of GLOF process chain, including initial mass movement from mother glacier and lateral moraine slope, displacement wave generation and propagation in the lake, overtopping flow and erosion on moraine dam and subsequent downstream flooding were simulated. This study will help the local government understand the potential hazards of Bienong Co and serve as a reference for other scholars studying glacial lakes and GLOFs in the SETP region.

2 Study area

Bienong Co is located in the upper area of Yi'ong Zangbo (Zangbo means river in Tibetan) watershed (30˚05' - 31˚03'N, 92˚52' - 95˚19'E) in the SETP (Fig. 1a). As a one-level tributary of the Parlung Zangbo and a two-level tributary of the Yarlung Zangbo (i.e., the Brahmaputra River), the Yi'ong Zangbo drains an area covering 13,533 km^2. The terrain is high in the west and low in the east with high mountains and valleys. The climate is warm and humid, featuring the mean annual precipitation of 958 mm and mean annual temperature of 8.8 ℃ (Ke et al., 2013, 2014). There were 1,907.76 km^2 glacier coverage, 105 moraine-dammed glacial lakes with a total area of 16.87 km^2 in 2016 (Duan et al., 2020). Seven glacial lakes in the watershed, including Bienong Co, were considered to have high GLOFs potential (Duan et al., 2020), of which, the Jinwu Co collapsed on June 26, 2020 (Zheng et al., 2021). As of 2021 there have been three recorded large GLOF events in the basin, all of which caused very significant damage to the infrastructures in downstream region (Sun et al., 2014; Yao et al., 2014; Zheng et al., 2021) (Fig. 1b). Bienong Co is an end moraine-dammed lake constrained by the snout of the mother glacier (Mulang Glacier) on the south and a massive unconsolidated terminal moraine dam on the northwest (Fig. 1c). The water surface height in 2021 is 4745 m covering an area of 1.15 ± 0.05 km^2 that has remained generally stable since 1988. Mulang Glacier has an area of 8.29 ± 0.22 km^2 and mean surface slope of ~18.28˚, which has also remained largely unchanged area over the last 45 years. However, the glacier ablation zone experienced a thinning of 6.5 m/year. The flow of Bienong Co converges into Xiong Qu (Qu means river in Tibetan) which is one of the two main tributaries of the upper Yi'ong Zangbo (Fig. 1b). The flow channel from the Bienong Co to the confluence of Xiongqu and Songqu Co (another main tributary of the upper Yi'ong Zangbo) stretches ~53 km, with the river longitudinal drop ratio of 14.48‰. There are 18 settlements and 13 bridges densely distributed along the flow channel, as well as a large amount of agricultural land. In addition, the Jiazhong Highway extends closely along the river (Fig. 1d).

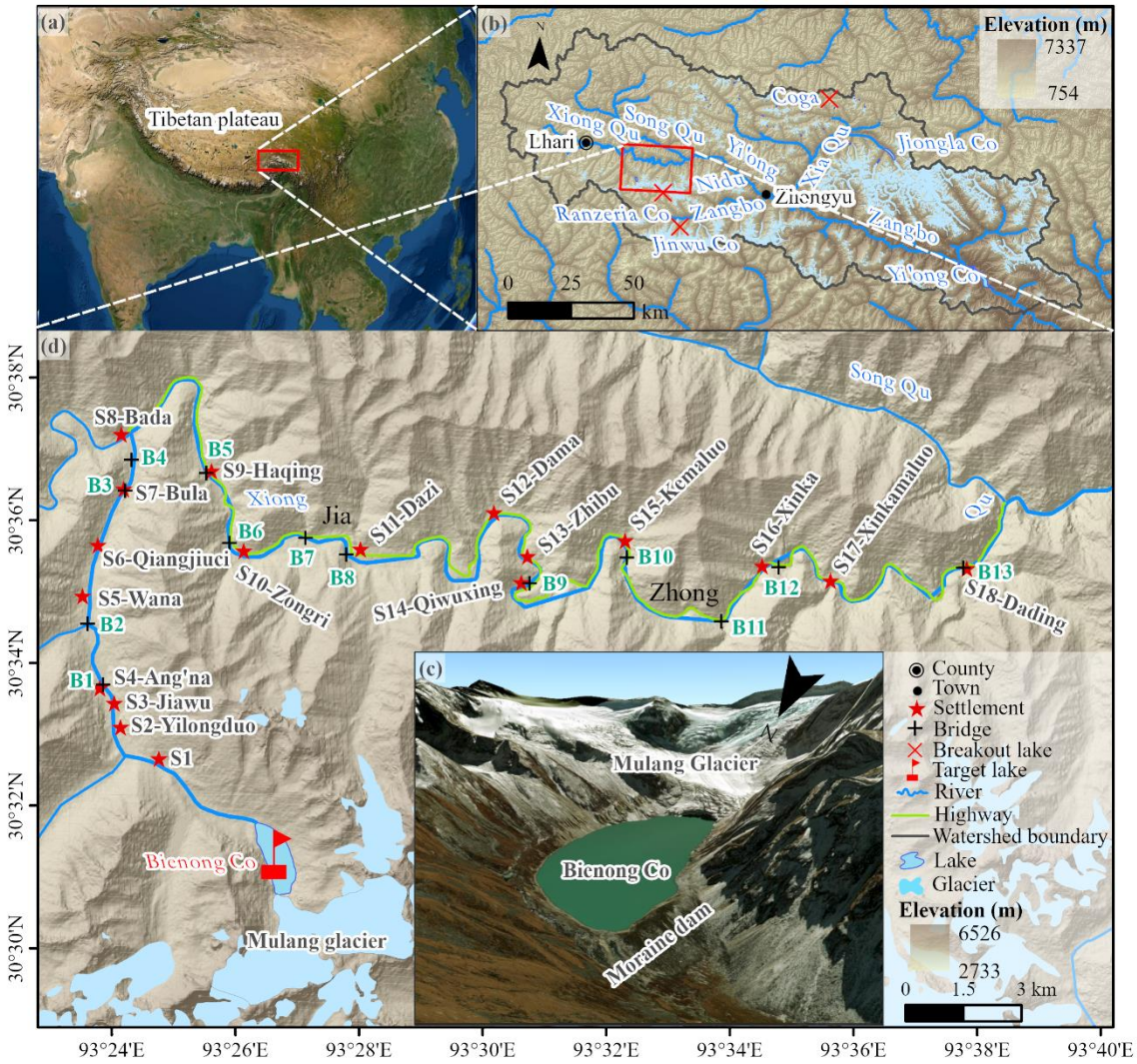

Figure 1. The overview of the study area. (a) The location of Yi'ong Zangbo watershed, (b) the location of Bienong Co, (c) the close view of Bienong Co, and (d) distribution of settlements as well as bridges within ~53 km downstream Bienong Co. Background of Fig. 1a and c is the MapWorld image, based on which, settlements, bridges and Jiazhong Highway along the flow channel were identified. Background of Fig. 1b and d is the Advanced Land Observing Satellite's (ALOS) mission Phased Array type L-band Synthetic Aperture Radar (PALSAR) Digital Elevation Model (DEM).

The area of Bienong Co has remained basically stable in the past 40 years, but it's area of 1.15 ± 0.05 km^2 in 2021 is almost twice the size of the two nearby failure glacial lakes, one is Jinwu Co (Zheng et al., 2021) and the other is Ranzeria Co, which is located just 9 km southeast of Bienong Co (Sun et al., 2014). The moraine dam of Bienong Co has an average height of 72 m, enclosing a water volume of 65.2×10^6 m^3, accounting for 64% of the total (Fig. 2e). The greater the volume of water retained in the lake, the greater the volume of water available for potential flooding (Westoby et al., 2014), and the greater the hazard caused by GLOFs. GLOFs are extremely complex phenomena, each of them is a distinctly unique event with the characteristics determined by the triggering mechanism, lake hypsometry, the geometry, composition, and structural integrity of the moraine dam, as well as the topography and geology of the flood path (Westoby et al., 2014). Studies of history GLOFs reveal that the most common cause of glacial lakes' failure in the Himalaya is mass movement (snow, ice, and/or rock) entering lakes (Richardson and Reynolds, 2000; Wang et al., 2012; Emmer and Cochachin, 2013; Worni et al., 2014) and subsequently overtopping and eroding the moraine dam (Risio et al., 2011). Bienong Co is directly connected to Mulang Glacier whose ablation zone that is defined as the mother glacier tongue (MGT) in this study has an average slope of 20˚ with well-developed ice crevasses (Fig. 2a and b). Lv et al., (1999) proposed that a slope of MGT greater than 8˚ is conducive to the occurrence of ice avalanche. In the context of global warming, glacial meltwater can lubricate the glacier itself, increasing the likelihood of

overhanging ice sliding into the lake (Wang et al., 2015). Therefore, ice disintegration from the Mulang Glacier could be a potential trigger for GLOFs of Bienong Co. In addition, the GLOF of Jinwu Co, a moraine dammed glacial lake located about 24 km to the southeast of Bienong Co, was caused by an initial moraine landslide with slope range of 30˚ - 45˚ on the left side (Zheng et al., 2021). Bolch et al. (2011) and Rounce et al. (2016) both deemed that non-glacierized areas around a lake with a slope > 30° are potential rock fall, landslide, or other solid mass movement region. There are multi locations with lateral moraines around Bienong Co that fit into this slope range (Fig. 2c, d and e). Thus, lateral moraine landslides could also be a potential trigger for Bienong Co's GLOF.

Dam characteristics, such as dam geometry (freeboard, width to height ratio, distal face slope), dam material properties, ice-cored moraine conditions govern the stability of the dam (Huggel et al., 2004; Prakash and Wang et al., 2011a; Nagarajan, 2017). Freeboard refers to the vertical distance between the lake level and the lowest point on the dam crest, which reflects the minimum wave amplitude needed for the occurrence of the overtopping, and a higher freeboard is not conducive to the occurrence of overtopping (Emmer and Vilímek, 2014). A natural outlet with a width of ~50 m in the right of the dam (facing downstream) (Fig. 2e and f), indicating the freeboard of Bienong Co is 0 m, which signals the high potential overtopping of the lake. The moraine dam is 550 m wide and the height is variable with an average height of 72 m and the width-height ratio of 7.64 (Fig. 2e). According to the thresholds favoring GLOFs of dam width smaller than 60 m proposed by Lv et al. (1999), width-height ratio smaller than 0.2 proposed by Huggel et al. (2004), the moraine dam of Bienong Co is stable. However, freeboard of 0 m and the distal facing slope of 35˚ are the conditions conducive to GLOFs based on the favoring thresholds of smaller than 25 m (Mergili et al., 2011) and larger than 20˚ (Lv et al., 1999). The moraine dam of Bienong Co is covered with vegetation, the surface layer is a larger particle size of the stone, below the smaller particle size, the material is loose and poorly cemented, which is susceptible to destruction by water forces (Fig. 2e). The existence of ice core inside the moraine dam is unknown, but there is no ice core in Jinwu Co's breached dam. The dam crest elevation of Bienong Co is 320 m higher than that of Jinwu Co. Additionally, McKillop and Clague (2007) argued that moraines with rounded surfaces and minor superimposed ridges are considered ice-cored, whereas narrow, sharp-crested moraines with angular cross-sections are interpreted as ice-free, and the dam of Bienong Co clearly fit the latter category. In summary, we consider that the potential threats to Bienong Co are mainly from its mother glacier's ice avalanches and lateral moraine landslides.

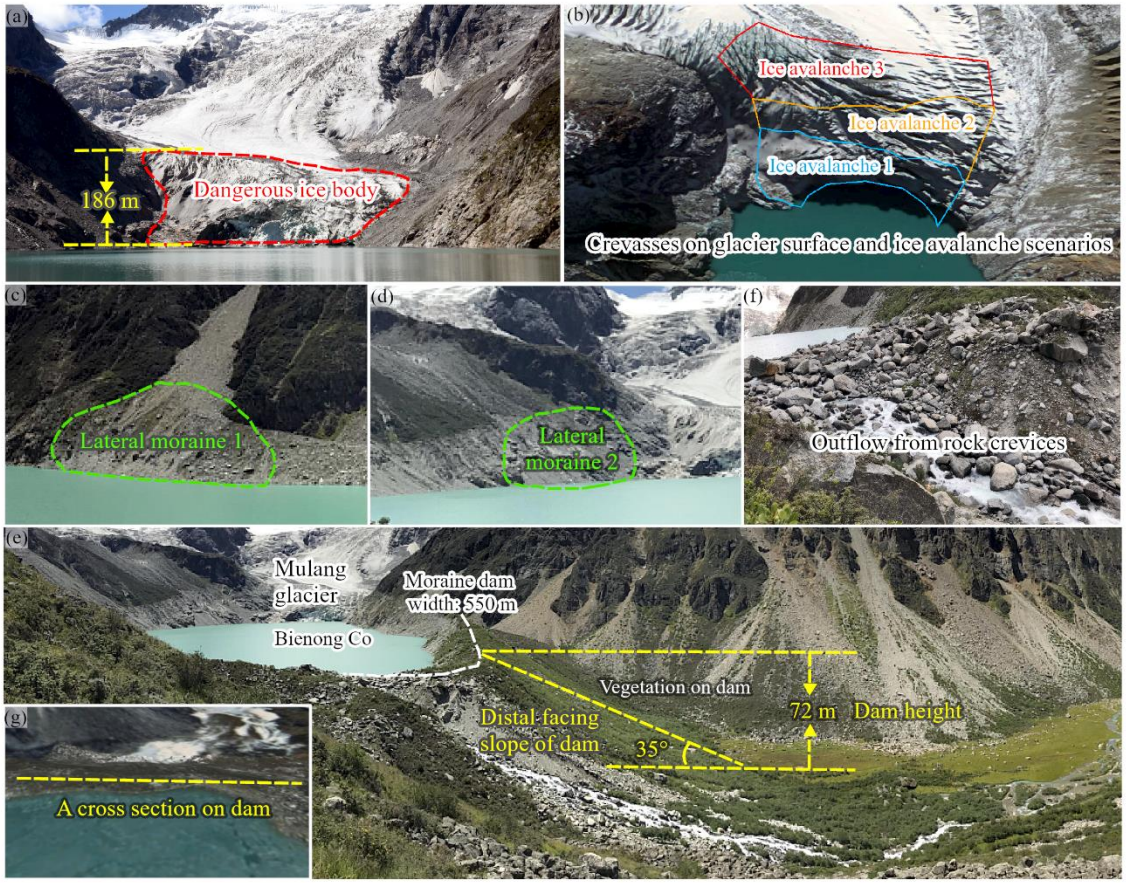

Figure 2. The hazards assessment of Bienong Co. (a) The connection condition of Mulang Glacier and Bienong Co, (b) the crevasses on glacier surface and the assumed ice avalanche scenarios of Mulang Glacier, (c) and (d) the assumed lateral moraine location, (e) and (f) the moraine dam of Bienong Co, and (g) a cross section on the moraine dam for statistic.

3 Methodology

3.1 Bathymetry and modeling

Lake bathymetric information is one of the most important inputs in the dynamic modeling of GLOFs, which can accurately reflect the topography of the lake basin below the water surface and be used to calculate the potential flood volume released in different breach scenarios (Westoby et al., 2014). In this study, the depth data were obtained by a USV (APACHE 3) system, which consists of four main parts, i.e., the data acquisition module, the data transmission module, the positioning and navigation control module, and the power module (Li et al., 2021) (Fig. 3a and b). The USV system has a draft of 10 cm, which is smaller than the inflatable kayak used in previous studies (Haritashya et al., 2018; Sattar et al., 2019, 2021). The D230 Single-Frequency Depth Sounder mounted on the USV is designed the measure range of 0.15 - 300 m with the depth resolution of 1 cm and the bathymetry error of ± 1 cm + 0.1%×h (water depth). The sounder can operate at 200 kHz and water temperature range of -30℃ - 60℃, meanwhile a real-time kinematic system enables a precise positioning for the bathymetric position with the horizontal error of ± 8 mm, the vertical error of ± 15 mm and the directional error of 0.2˚ on the 1 m baseline. Field measurements were carried out on August 27, 2020. We designed four longitudinal routes and 13 transverse routes prior to the survey, along which the USV based measurement was conducted (Fig. 3c). The maximum speed of USV can reach 8 m/s, our survey was conducted with a speed of 2 m/s for a total route of 22.58 km in the Bienong Co. Due to absence of any obstructions on the lake, such as ice or small islands, the high performance of the USV and the real-time monitoring, the survey was accurately completed along the designed route. A total of 16,020 valid sounding points basically covering the entire glacial lake were measured, which well fulfilled the data density requirement to model the lake basin

topography (Fig.3c).

Bathymetric map was created within ArcGIS Pro software using natural neighbor interpolation algorithm (Thompson et al., 2016; Haritashya et al., 2018; Watson et al., 2018). In addition, Surfer software was used to simulate the 3D morphology of the Bienong Co's lake basin. Lake capacity can be understood as the volume of water storage below a certain water level, which is the volume between a certain spatial curved surface and a certain horizontal surface (Shi et al., 1991). In this study, the volume of Bienong Co was obtained by multiplying the depth data and map resolution (5 m) as Eq. (1):

$$V = \sum_{i=1}^{n} H_i \cdot \lambda \tag{1}$$

where V is the volume (m^3) of Bienong Co; H_i is the depth (m) at *i-th* pixel; n is the number of the pixels in the lake area; λ is the pixels resolution (m^2) of the bathymetric map.

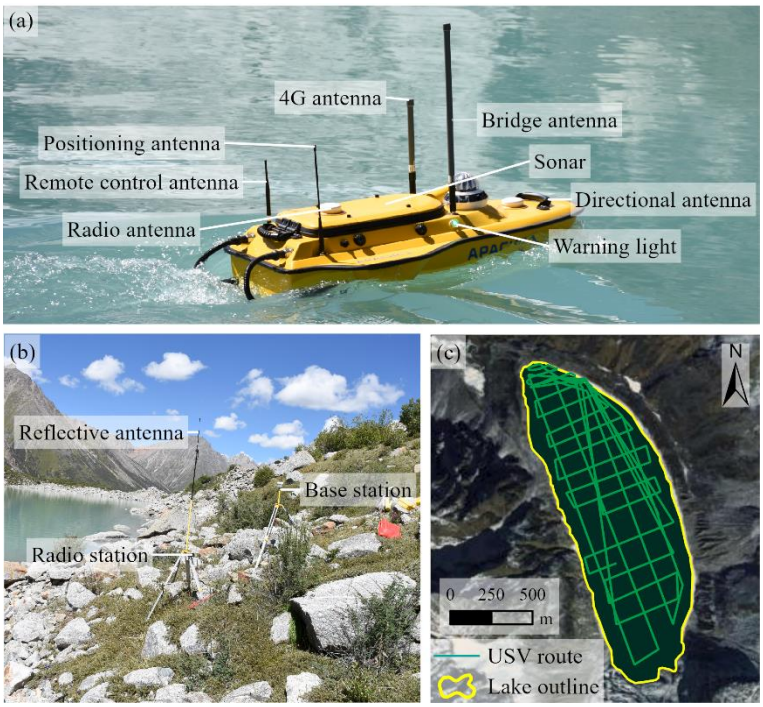

Figure 3. The bathymetry of Bienong Co. (a) the USV sampling equipment in water, and (b) on land; (c) the sampling path of USV on Bienong Co covering the base map of MapWorld image. Photos taken by Xiaojun Yao on August 27, 2020.

3.2 Potential GLOF modeling

Emmer and Vilímek (2013, 2014) and Haeberli et al. (2001) suggested that the assessment of glacial lake hazards should be conducted based on a systematic and scientific analysis of lake types, moraine dam characteristics, eruption mechanisms, downstream processes in the river valley and possible process cascades. The methodology used in this study refers to the GLOFs process chain proposed by Worni et al. (2014), which has been employed by Somos-Valenzuela et al. (2016) and Lala et al. (2018) to study Imja Tsho in Nepal and Palcacocha and Huaraz lakes in Peru, respectively. And in this study, we aim to depict potential GLOFs induced by ice avalanches originate from the Mulang Glacier (Fig. 2a and b) and landslides from lateral moraine (Fig. 2c and d) and assess the potential inundation in the downstream region. The wave resulted from material entering Bienong Co might overtop the moraine dam and initiate an erosive breaching process, releasing considerable amounts of water and debris into the downstream flow channel (Somos-Valenzuela et al., 2016). Three model were used to simulated the GLOFs process chain, RAMMS model was used for simulation of potential mass movement (Christen et al., 2010), BASEMENT model was used to simulate the displacement wave in the lake, Heller-Hager model was used as a calibration for BASEMENT's results, and BASEMENT model was also adopted to simulate the dynamic breaching process of moraine dam, the propagation of flood wave and the inundation in downstream. In next sections, simulation methods for ice avalanches and landslides, displacement wave in lakes, overtopping flow and erosion on moraine dam, and downstream inundation were

described.

3.2.1 Triggers determination and simulation

Ice avalanches are the most common GLOFs trigger in the Tibet in China (Yao et al., 204; Liu et al., 2019). Mass movements into lakes generate impulse waves that may produce overtopping flow scouring and eroding moraine dams, or disrupt the hydrostatic pressure-bearing capacity of moraine dams. Based on a survey of the environment surrounding Bienong Co, ice avalanches from Mulang Glacier and two locations of lateral moraine landslide were selected as potential triggers for GLOFs. Wang et al., (2012) defined the volume of dangerous glacier as the volume from the location of abrupt changing slope to the glacier termini or the volume of glacier snout where ice cracks are well developed. We adopted the latter, i.e., the crevasse-developed ice body of Mulang Glacier shown in MapWorld image with a surface area of 0.19 km^2 as the potentially ice avalanche source of Bienong Co (Fig. 2a). For the convenience of subsequent description, we name it Scenario A. The elevation difference between the top of the dangerous ice body and the lake surface was measured to be about 155 - 208 m based on ALOS PALSAR DEM. We divided the dangerous ice body into three parts according to elevation range to simulate subsequence processes from ice avalanches of different magnitudes (ice avalanche 1, 2 and 3 in Fig. 2b,). Scenario A1 was defined as a low-magnitude trigger, ice body at elevation below 4,844 m yields a release area of 0.05 km^2 with the maximum and average elevation differences of 99 m and 75.8 m from the lake surface. Scenario A2 was defined as a moderate-magnitude trigger, ice body at elevation below 4,889 m yields a release area of 0.11 km^2 with the maximum and average elevation differences of 144 m and 102.7 m from the lake surface. Scenario A3 was defined as an extreme-magnitude trigger, the total ice body of crevasse with an area of 0.19 km^2 was set as a release area, with the average elevation difference between glacier surface and lake surface of 131 m. In the above three cases, we assumed that the release depths of ice avalanches are the average elevation differences from the glacier surface to the lake surface, i.e., the calculation is based on the assumption that the glacier is supported by flat bedrock located at the height of the lake water table.

Lateral moraine landslide as a GLOFs trigger is not common on the Tibetan Plateau, but the GLOF of Jinwu Co in 2020 was caused by a lateral moraine landslide (Liu et al., 2021; Zheng et al., 2021), therefore it was taken as a trigger of the potential GLOF for Bienong Co. Two areas of lateral moraine within the slope range of 30˚ - 45˚ were selected as potential landslide sites, one is located on the left bank (in this study, the left and right sides are defined in a downstream-oriented manner) of Bienong Co, near the moraine dam with an area of 0.015 km^2, we named it Scenario B. Another is located on the right bank, near the mother glacier with an area of 0.024 km^2, we named it Scenario C. Two sites are at different distances from the moraine dam and we set three different release depths of 2 m (Scenario B1 and C1), 5 m (Scenario B2 and C2), and 10 m (Scenario B3 and C3) for each release area as low-, moderate- and extreme-magnitude trigger. Therefore, a total of two different types, three different locations and nine different magnitudes of materials were designed to enter the lake as potential triggers for GLOFs in this study. The above design fully considers the impact of triggers on Bienong Co under different magnitudes, and the results are used as the input for the subsequent disaster chain simulation.

In this study, ice avalanches and lateral moraine landslides of Bienong Co were modeled using the Avalanche module of RAMMS model (Barteltet al., 2013), which has been successfully used for simulating triggers of GLOFs (Somos-Valenzuela et al., 2016; Lala et al., 2018; and Sattar et al., 2021). RAMMS adopts the Voellmy-Salm finite volume method to solve the depth-averaged equations governing mass flow in two dimensions (Christen et al., 2010). Based on the basic inputs of DEM, the initial release area and depth, the calculation domain, and the friction parameters μ (the velocity-independent dry Coulomb) and ξ (velocity-dependent turbulent friction terms), the outputs of runout distances, flow height and flow velocity can be calculated. And time series of material entering the glacial lake can serve as the input condition for subsequent simulations. For this study case, the initial release area was determined by combining MapWorld image of the spatial resolution of 0.5 m (https://www.tianditu.gov.cn/) and ALOS PALSAR DEM with a spatial resolution of 12.5 m (https://asf.alaska.edu/data-sets/derived-data-sets/alos-palsar-rtc/alos-palsar-radiometric-terrain-correction/), the latter is also the basic data for RAMMS

and BASEMENT models. Values of μ=0.12, ξ=1,000 m s^{-2}, and ρ=1,000 kg m^{-3} for ice avalanche and ρ=2,000 kg m^{-3} for landslide were used, which agree with values used in previous GLOF-producing avalanche models (Schneider et al., 2014; Somos-Valenzuela et al., 2016).

3.2.2 Hydrodynamic wave simulation

Processes following mass movement entering the lake, such as the generation and propagation of displacement wave, the overtopping flow and erosion on moraine dam, and the inundation of downstream were modeled using BASEMENT model v2.8.2 (Vetsch et al., 2017), developed by the Laboratory of Hydraulics, Glaciology and Hydrology (VAW), ETH Zurich. BASEMENT is both a hydrodynamic model and a sediment transport model, making it well suited to model much of the GLOF process chain (Worni et al., 2014). It solves 2-D shallow water equation (SWE) in combination with sediment transport equations, primarily the Shields parameters and the Meyer-Peter and Müller (MPM) equations (Shields, 1936; Vetsch et al., 2017). The simulation of hydrodynamic waves in the lake is performed using the 2D modeling of BASEMENT based on unstructured grids. The BASEmesh plugin for QGIS (QGIS Development Team, 2016) developed by BASEMENT greatly facilitates the generation of mesh. The lake bathymetry data were produced into DEM with a spatial resolution of 5 m using ArcGIS Pro software for reflecting the lake basin topography. The triangular irregular network (TIN) within the lake area was set to a maximum area of 500 m^2 to simulate the generation and propagation of hydrodynamic waves in the lake effectively and accurately. The input boundary conditions are time series of ice avalanches and landslides generated by RAMMS model. In each time period, RAMMS calculates the total amount of sediment, and the inflow rate can be determined by calculating the difference of sediment entering the lake at the two time points. Pure rock landslides have been studied with densities ranging from 1,950 kg m^{-3} to 2,200 kg m^{-3} (Wang et al., 2017), and most ice-dominated avalanches have densities of about 1000 kg m^{-3}. In this study, the ice avalanche density was set as 1,000 kg m^{-3} and the landslide density is set to 2,000 kg m^{-3}. Since BASEMENT only accepts water as an inflow, this difference due to density is considered by expanding the landslide material entry rate by a factor of two (namely, 1,000 kg m^{-3} of water is equivalent to 1,000 kg m^{-3} of ice avalanche volume, and only 500 kg m^{-3} of landslide material), which is the usual approach used in the simulation process (Byers et al., 2018 and 2020).

It was shown that the 2D SWE used by BASEMENT model inherently leads to excessive wave attenuation. Heller-Hager model (Heller et al., 2009) is a combination of analytical and empirical equations used to simulate impulse wave generation, propagation, and run-up from the movement of material entering a lake. Although the approach relies on simplifying measurements about lake geometry, it has been used to successfully simulate multi real events and performs well in characterizing impulse waves within lakes, making it a simple but useful calibration measure for more complex hydrodynamic models (Somos-Valenzuela et al., 2016). BASEMENT simulated waves are usually considered more accurate when they are of the same order of magnitude as Heller-Hager waves; however, when they are not, the mass entry rate is varied by adjusting the inflow hydrograph and boundary width to match the amplitude of Heller-Hager empirical model near the dam of the initial wave trajectory (Lala et al., 2018). The Heller-Hager model simulates waves in two cases: (a) with longitudinal impacting slide and confined transverse wave propagation and (b) with the slide impacting across the reservoir and completely free radial wave propagation. In present study, ice avalanches belong to case (a), and landslides belongs to case (b). Compared to case (a), the impulse wave (its amplitude and energy) in case (b) decreases more rapidly because it propagates over a larger area is accompanied by wave refraction and reflection.

3.2.3 Moraine dam erosion simulation

The abnormally high lake outflow is sufficient to destroy the surface protection layer of the outlet streambed and trigger vertical dam erosion. After the initial cut, more lake water was able to flow out, followed by an increase in sediment transport rate and a gradual widening of the rift. In this study, the hydro-morphodynamic simulations of potential erosion-driven breach failures

of Bienong Co was carried out by BASEMENT model, which uses the Meyer-Peter and Müller (MPM) equation to characterize sediment transport and estimates suspended and nudged mass fluxes by calculating the shear stress in the flow through the modified Shields parameter (Vetsch et al., 2017). The overtopping flow leading to erosion of the moraine dam is generated by the wave amplitude of the BASEMENT model calibrated by the Heller-Hager model. In the previous step, we adjusted the wave amplitude near the moraine dam in the BASEMENT model to be close to (difference within 1 m) that calculated by Heller-Hager model by modifying the width of the upstream boundary. ALOS PALSAR DEM is the base data for the mesh generation of moraine dam with the maximum TIN area of 200 m^2. We set a cross section along the crest of moraine dam (Fig. 2g), where the moraine dam deformation, i.e., erosion, and the overtopping as well as outflow discharges were analyzed. BASEMENT model provides both single-grain (MPM) and multi-grain (MPM-multi) algorithms to simulate material transport. The MPM-Multi model simulates hiding and armoring processes that may lead to unrealistically low levels of erosion (Vetsch et al., 2017). The MPM model ignores these processes, however, it can lead to an overestimation of erosion. In this study, we applied the MPM-multi model to simulate the bedload transport of moraine dam, which are composed of materials with different grain sizes. The specific grain size distribution was not measured, it was instead taken from an inventory of glacial lakes in the Indian Himalaya (Worni et al., 2013) that had performed well in recreating previous GLOFs in Nepal (Byers etal., 2020). Despite uncertainty in the actual grain size distribution, a similar GLOF modeling study in the Barun Valley (Byers etal., 2018) found little difference in simulated moraine erosion between the grain size distributions listed in Worni et al. (2013). The moraine dam of Bienong Co consists of a large grain cover with a thickness of about 0.5 m at the top and fine grain underneath, which is clearly visible on the side walls of the channel scoured by water (Fig. 2e). We set up two soil layers in BASEMENT model to represent the above situation. The largest particle size (d_{50} = 180 mm) in the upper layer with a depth of 0.5 m, while the grain size distribution of lower layer that has a depth of 71.5 m (considering the mean height of moraine dam of 72 m) is consistent with Worni et al. (2013). Finally, a correction factor of 2.0 was used in model to increase the rate of bed load transport. Values between 0.5 (low transport) and 1.7 (high transport) are generally realistic (Wong and Parker, 2006), while a value of 2.0 provides high sediment transport conditions (Somos-Valenzuela et al., 2016) to compensate the lower erosion of MPM-multi model.

3.2.4 Downstream impact analysis

The flow channel from Bienong Co to the convergence with Song Qu stretches ~53 km (Fig. 1d), along which 18 settlements, 13 bridges and Jiazhong Highway are distributed. In this study, BASEMENT model was used to simulate Hydrodynamic behavior of potential GLOFs along the flow channel, and the hazard of floods was assessed by analyzing the inundation area, flow velocity, and flood arrival time at these settlements. The 2D model for an unsteady hydraulic simulation requires input of terrain data and boundary conditions. The terrain data was represented by a 2D mesh covering the entire flow area, which was obtained from ALOS PALSAR DEM. The mesh was also generated by the BASEmesh plugin of QGIS software, and the individual cell area for main flow channel and other regions were set to 500 m^2 and 5,000 m^2 considering the accuracy requirements of the simulation and the computational efficiency of the model. Friction of the river channel to a given flow is determined by the Manning's roughness coefficient (Coon, 1998), which is dependent on the land use and land cover of the modeling river channel in the study area. In this study, the GLC10 LULC product (http://data.ess.tsinghua.edu.cn/fromglc10_2017v01.html) with a spatial resolution of 10 m was used to obtain the value of Manning's N in the flow channel. The upstream boundary is the outflow hydrograph from the moraine dam simulated by BASEMENT model. And the downstream boundary is the water level-discharge relationship of the cross-section in downstream boundary of the simulation area, it was estimated by the critical depth method (Byers et al., 2018).

4 Results

4.1 Morphology and water storage estimation of Bienong Co

The basin morphology of Bienong Co was modeled based on the TIN grid created by the field depth data (Fig. 3). Apparently, this lake has a relatively flat basin bottom and both deep flanks (Fig. 4). Similar to most glacial lakes (Yao et al., 2012; Zhou et al., 2020), the slope of the lake shores near the glacier is steeper than that near the moraine dam. The water depth profile from moraine dam to mother glacier show that the depth of the lake reaches a maximum of 181 m at about 1,000 m from the moraine dam, corresponding to the slope of 11.3˚. The depth keeps stable at distance of 1,000 m to 1,500 m from the moraine dam, and the distance from the mother glacier to the deepest point of the lake is 600 m with the slope of 16.5˚. A depth profile facing the moraine dam from the left bank to the right bank shows that the left side is steeper than the right side. The glacial lake reaches its deepest point at 200 m from left shore with the slope of 43.4˚, then maintains flat to 430 m, and the distance between the bottom and right shore is 273 m with the slope of 32˚. The volume of Bienong Co, calculated using the surface elevation and the lake bed derived from the TIN grid, was about 102.3×10^6 m^3 in 2020, which is a generally accurate estimate of the magnitude of this moraine-dammed lake.

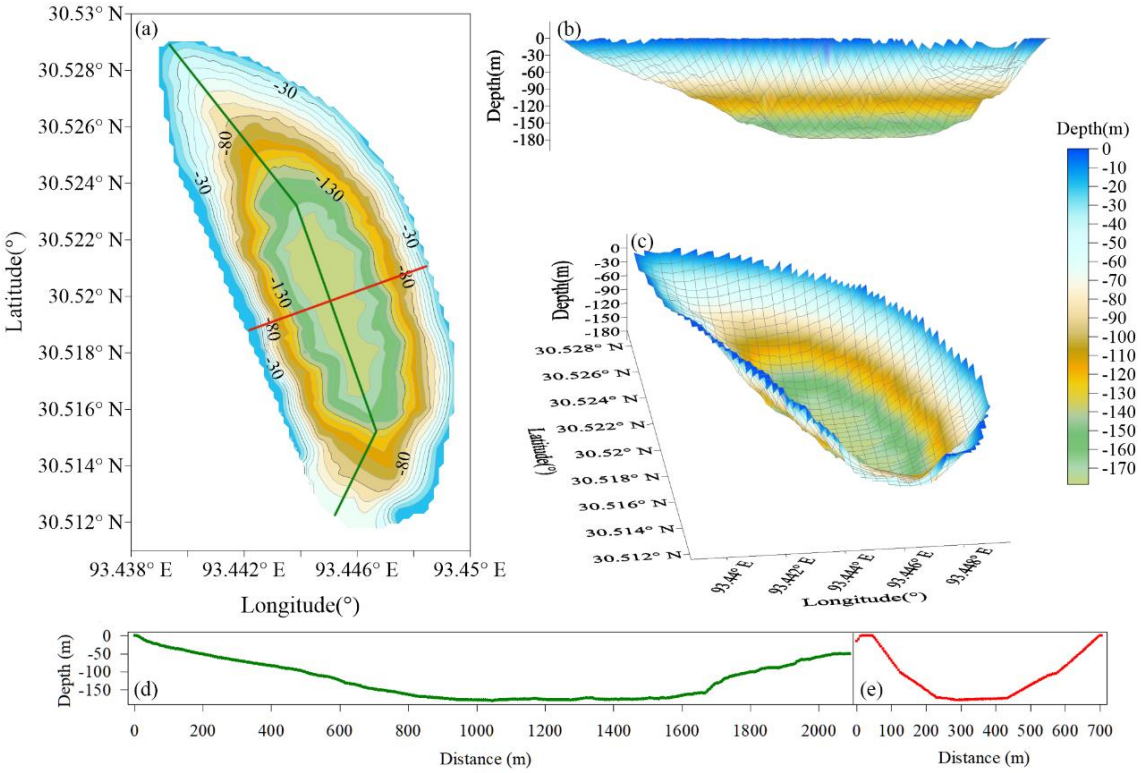

Figure 4. Morphology modeling of Bienong Co in 2020 and the equal-scale profiles of distance and depth from the moraine dam to Mulang Glacier (green line) and from the left shore to right shore (red line).

4.2 Potential GLOFs modeling

4.2.1 Ice avalanche and lateral moraine landslide

As calculated by RAMMS, the volume of ice avalanches entering Bienong Co for Scenarios A1, A2, A3 are 3.8 × 10^6 m^3, 4.9 × 10^6 m^3 and 5.8 ×10^6 m^3 (Fig. 5a). Most of materials enter the lake within about 120 s. Based on the area of ~1.15 km^2 in 2021, above three scenarios could result in a rise of about 3.3 m, 4.2 m and 5.1 m in the lake surface. Materials volumes entering the lake by both landslides are much smaller than that of the ice avalanche (Fig. 5b and c). Scenarios B1, B2, B3 and C1, C2, C3 dump 0.03 × 10^6 m^3, 0.09 × 10^6 m^3, 0.17 × 10^6 m^3, and 0.06 × 10^6 m^3, 0.15 × 10^6 m^3, 0.30 × 10^6 m^3 of material into the lake, respectively. The time for materials entering the lake is less than in Scenario A, with Scenario B1/2/3 being completed in about 10 s and Scenario C1/2/3 in about 15 s.

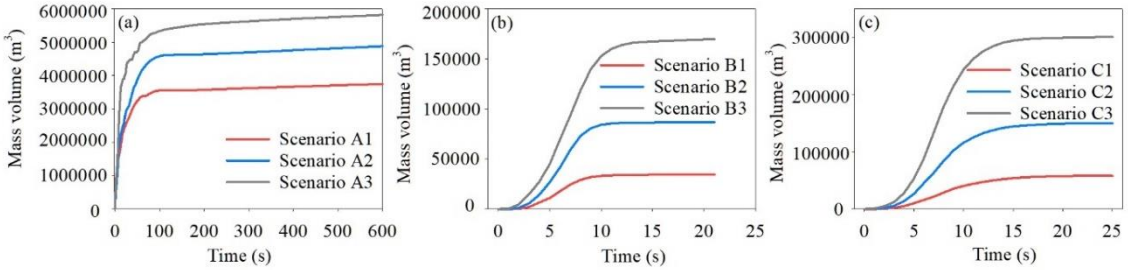

Figure 5. Volume of material entering Bienong Co for different (a) ice avalanches and (b), (c) landslide scenarios.

The impact area caused by material entering the lake differs for different scenarios. The impact zones caused by Scenarios A1, A2 and A3 are 0.27 km^2, 0.31 km^2 and 0.38 km^2, respectively, with horizontal distances of 549 m, 629 m and 752 m from the upper boundary (Fig. 6). In contrast, each of the three scenarios for Scenarios B and C result in a relatively small impact zone, with Scenario C3 being the largest of 0.14 km^2 and Scenario B1 being the smallest of 0.04 km^2. Scenarios A1, A2, and A3 produce maximum flow heights of 39.5 m, 46.2 m, and 53.5 m, and average flow heights of 12.2 m, 14.6 m, and 12.3 m in the impact area, respectively. The maximum flow height range for Scenario B1/2/3 is 6.8 - 14.6 m and the average flow height range is 1.8 - 3.5 m. The maximum and average flow height ranges for Scenario C1/2/3 are 5.7 - 29.2 m and 2.0 - 4.7 m (Fig. 6). The maximum flow velocities for Scenarios A1, A2 and A3 are 34.9 m/s, 43.1 m/s and 51.4 m/s, with the average flow velocities of 11.1 m/s, 12.3 m/s, and 16.8 m/s, respectively. The maximum and average flow velocities for Scenarios B1, B2 and B3 and C1, C2 and C3 are in the range of 21.3 - 33.6 m/s and 8.5 - 14.2 m/s, respectively (Fig. 6).

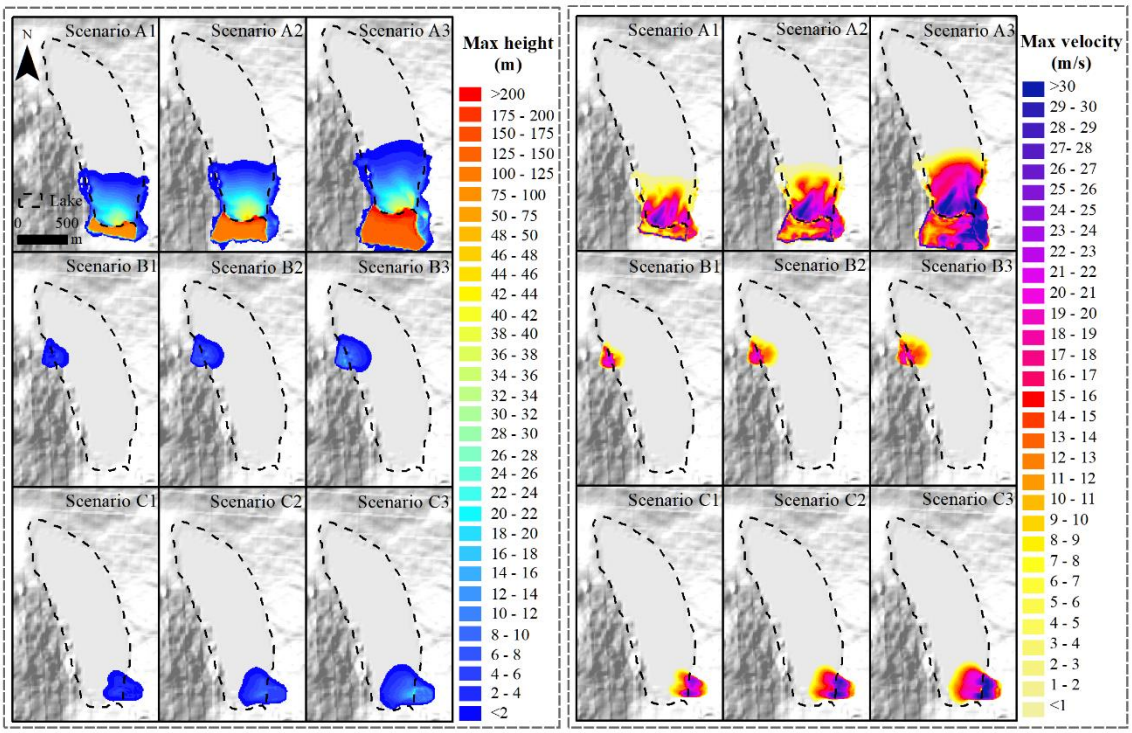

Figure 6. Maximum flow height (left) and maximum flow velocity (right) for different ice avalanches and landslides scenarios.

4.2.2 Generation and propagation of displacement wave

By counting material volumes of ice avalanches and landslides entering Bienong Co at different time periods based on RAMMS model, we derived the time series of the material entering rate as shown in Fig. 7. Compared to Scenarios A2 and A3, Scenario A1 has the highest peak flow rate of 439,952.57 m^3/s, but it decreases rapidly after reaching the peak within two seconds of the ice avalanche, i.e., the ice avalanche occurs in a moment. Scenarios A2 and A3 show obvious fluctuations in the process of ice avalanches into the lake, with sub-peaks in both scenarios that are comparable to the first peak, after which the flow rates still have strong fluctuations. The peak and sub-peak flow rate of Scenario A2 and A3 are 263,922 m^3/s, 238,086

m^3/s and 386,359 m^3/s and 373,449 m^3/s, both occurring at the 2nd and 8th seconds of the ice avalanche, respectively. This is because ice avalanches of Scenarios A2 and A3 are further away from the lake than Scenario A1, and total volumes of ice avalanches are larger than A1, so they entry into the lake undergo a more complex process. The process of landslide material entering the lake is simpler in Scenarios B and C. The peak flows increase sequentially form Scenarios B/C1, B/C2, to B/C3, with peak values of 50,849 m^3/s and 92,529 m^3/s for Scenarios B3 and C3, respectively. The peak flow for Scenario B3 is approximately 3.8 times that of B1, and it for Scenario C3 is 6.5 times that of C1, respectively. The peak flows for the six scenarios of Scenarios B and C occur in the range of 6th-8th seconds (Fig. 7).

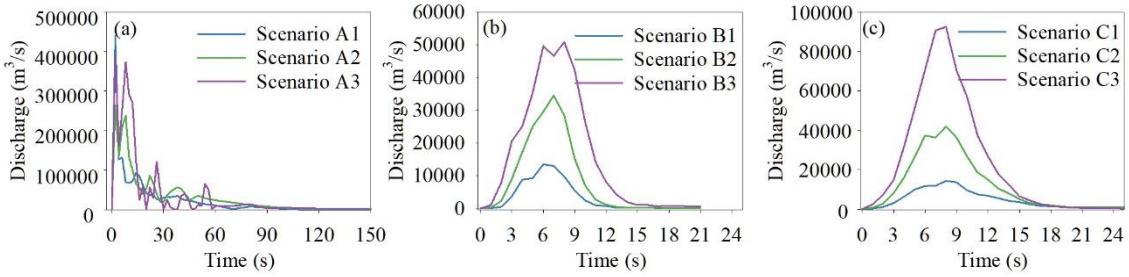

Figure 7. Time series of material entry into the lake for different ice avalanches and landslide scenarios.

The time-volume relationships of materials entering a lake have important effects on the generation and propagation of displacement waves in the lake. Ice avalanches scenarios (A1, A2 and A3) have a much greater impact on Bienong Co than two landslide scenarios (B1, B2, B3, C1, C2 and C3) because the assumed release volume of ice avalanche is much greater than that of landslides. The wave height near the moraine dam is the result of BASEEMNT model calibrated by the Heller-Hager model. By adjusting the inflow boundary's width, we made the BASEMENT model produce wave amplitudes near the dam with a difference smaller than 1 m of those calculated by the Heller-Hager model, which is important for subsequent simulations although the maximum wave amplitude in the lake is exaggerated.

In Scenario A, displacement waves propagate straight from the glacier to the moraine dam and arrive the vicinity of the moraine dam at about 70 s. Scenarios A1, A2 and A3 produce the highest wave amplitudes in the lake of 35.2 m, 39.0 m and 66.4 m, respectively, and the wave amplitudes near the moraine dam of 17.1 m (72 s), 20.2 m (74 s) and 25.2 m (72 s), respectively (Fig .8). Compared with Scenario A, wave amplitudes of Scenarios B and C are much lower. In Scenario B, a landslide occurs at the left shore of Bienong Co near the moraine dam (Fig. 2c). Displacement waves first propagate to the opposite shore along the perpendicular to the inflow boundary, and then they propagate to the moraine dam with the expansion. The maximum wave amplitudes in Bienong Co of Scenarios B1, B2, and B3 are 6.5 m, 14.1 m, and 18.0 m, respectively, and the wave amplitudes near the moraine dam are 1.2 m, 3.0 m, and 5.3 m, respectively (Fig. 8). The landslide in Scenario C occurs on the right bank of Bienong Co near the glacier, the same as Scenario B is that waves propagate to the opposite bank first after materials entering the lake, with the maximum wave amplitudes of 4.8 m, 9.6 m and 24.7 m for Scenarios C1, C2 and C3. Unlike Scenario B, displacement waves in Scenario C cross the entire lake reaching the moraine dam with wave amplitudes of 0.6 m, 2.2 m and 4.9 m near the moraine dam, respectively (Fig. 8). Therefore, although the landslide volume of Scenario C is larger than that of Scenario B, wave amplitudes near the moraine dam are smaller than those of Scenario B.

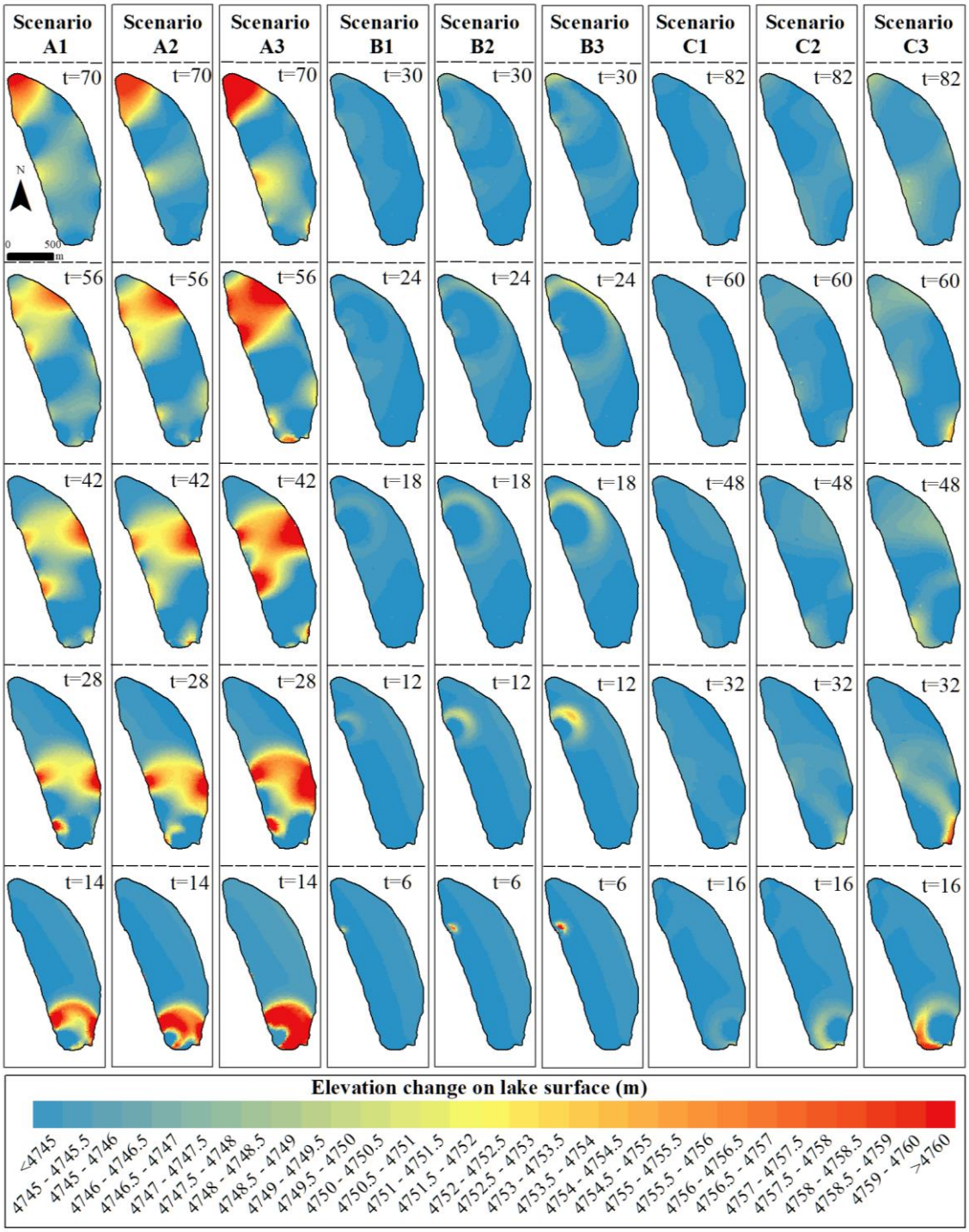

Figure 8. Propagation of displacement waves in the lake for different ice avalanches and landslide scenarios.

4.2.3 Overtopping flow and erosion on moraine dam

Since the freeboard of the moraine dam is 0 m, the occurrence of overtopping flow is inevitable in all scenarios, but there are differences in magnitude. In Scenarios A1, A2, and A3, peak discharges at breaches of moraine dam are 4,996 m^3/s, 7,817 m^3/s and 13,078 m^3/s corresponding to total released volume of 24.1 × 10^6 m^3, 25.3 × 10^6 m^3 and 26.4 × 10^6 m, respectively (Fig. 9). Discharges at the moraine dam stabilize after ice avalanches entering Bienong Co about 18,000 s, 10,800 s and 7,200 s, respectively. Therefore, the erosion of the moraine dam and the total volume of water lost in the lake were counted based on the above time points. Due to the huge discharge output, the moraine dam in Scenarios A1, A2, and A3 are eroded to form breaches. Due to the similar volume of released water, the depth of the breach is slightly different for Scenarios A1, A2 and A3, they are 19.0 m 19.1 m and 19.3 m, respectively (Fig. 10). While the peak discharge is much different for the three

scenarios, resulting in different breach widths of 295.0 m, 339.4 m, and 368.5 m. Scenarios B1, B2, B3 and C1, C2, C3 resulted in overtopping flows of 0.6 × 10^6 m^3, 1 × 10^6 m^3 and 2.6 × 10^6 m^3, as well as 0.1 × 10^6 m^3, 0.9 × 10^6 m^3 and 3.4 × 10^6 m^3, respectively, in which, only Scenarios B3 and C3 cause erosion of the moraine dam and form breach. Discharges at the breach become stable since 18,000 s following landslide material entry into the lake in Scenarios B3 and C3, with breach depths of 6.5 m and 7.9 m, respectively. And breach widths are 153 m and 169 m with the peak discharges of 504 m^3/s and 733 m^3/s.

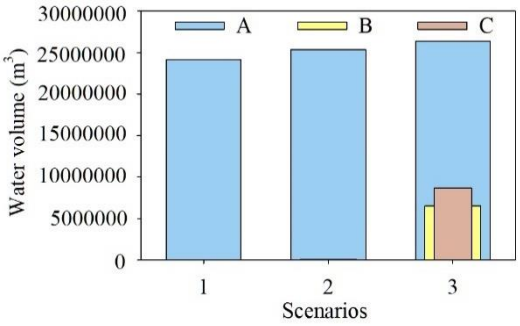

Figure 9. Discharge of water bodies in glacial lakes under different scenarios.

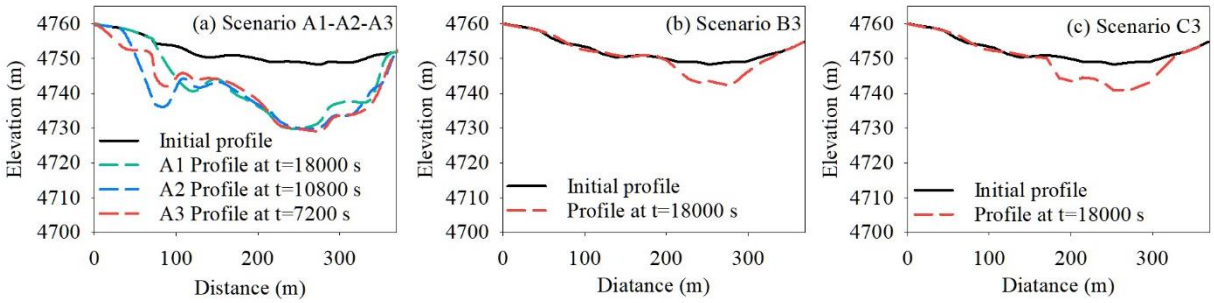

Figure 10. Erosion of moraine dams under different conditions at cross section in Fig. 2g.

4.2.4 GLOFs impact in downstream region

The hydraulic behavior of GLOFs in the flow channel that from the immediately downstream of moraine dam to the convergence with Song Qu with a distance ~53 km was simulated using BASEMENT model. Due to the lack of reliable data on small baseflows in the flow channel, they were neglected in the simulation. Considering the propagation of floods in different scenarios, we assessed the propagation of GLOF in the downstream channel within 20 hours from ice avalanche and landslide materials entry into the lake. Peak discharges at the breach outlet of Scenarios A1, A2 and A3 all occur about 600 s after the ice avalanche material enters the lake, they are 4,996 m^3/s, 7,817 m^3/s and 13,078 m^3/s, based on which, floods all pass through 18 settlements in the downstream river in 20 hours, with the inundation areas of 7.6 km^2, 8.0 km^2 and 8.5 km^2 as well as average water depths of 8.4 m, 9.1 m and 10.0 m, respectively (Fig. 11). The Scenarios B1 and C1 only have a small amount of overtopping flow from the lake (peak discharges of 106 m^3/s (after 40 s) and 12 m^3/s (after 50 s)), and fail to generate runoff downstream of the dam. Scenarios B2 and C2 produce very limited overtopping flow with peak discharges of 177 m^3/s (after 240 s) and 186 m^3/s (after 480 s), and outflows remain only within approximately 1 km downstream of the dam. Peak discharges at breach outlet of Scenarios B3 and C3 are 504 m^3/s (after 240 s) and 733 m^3/s (after 480 s), yielding inundation areas of 1.7 km^2 and 2.2 km^2 with average water depths of 1.9 m and 2.4 m in the downstream region. Both GLOFs pass through first eight settlements, but the flood of Scenario C3 flows farther (Fig. 11). Among the nine scenarios we assumed, only Scenarios of A1, A2, A3, B3 and C3 caused GLOFs propagation in the downstream region with a far distance, in which Scenario A3 had the largest flood magnitude, and Scenario B3 had the smallest magnitude.

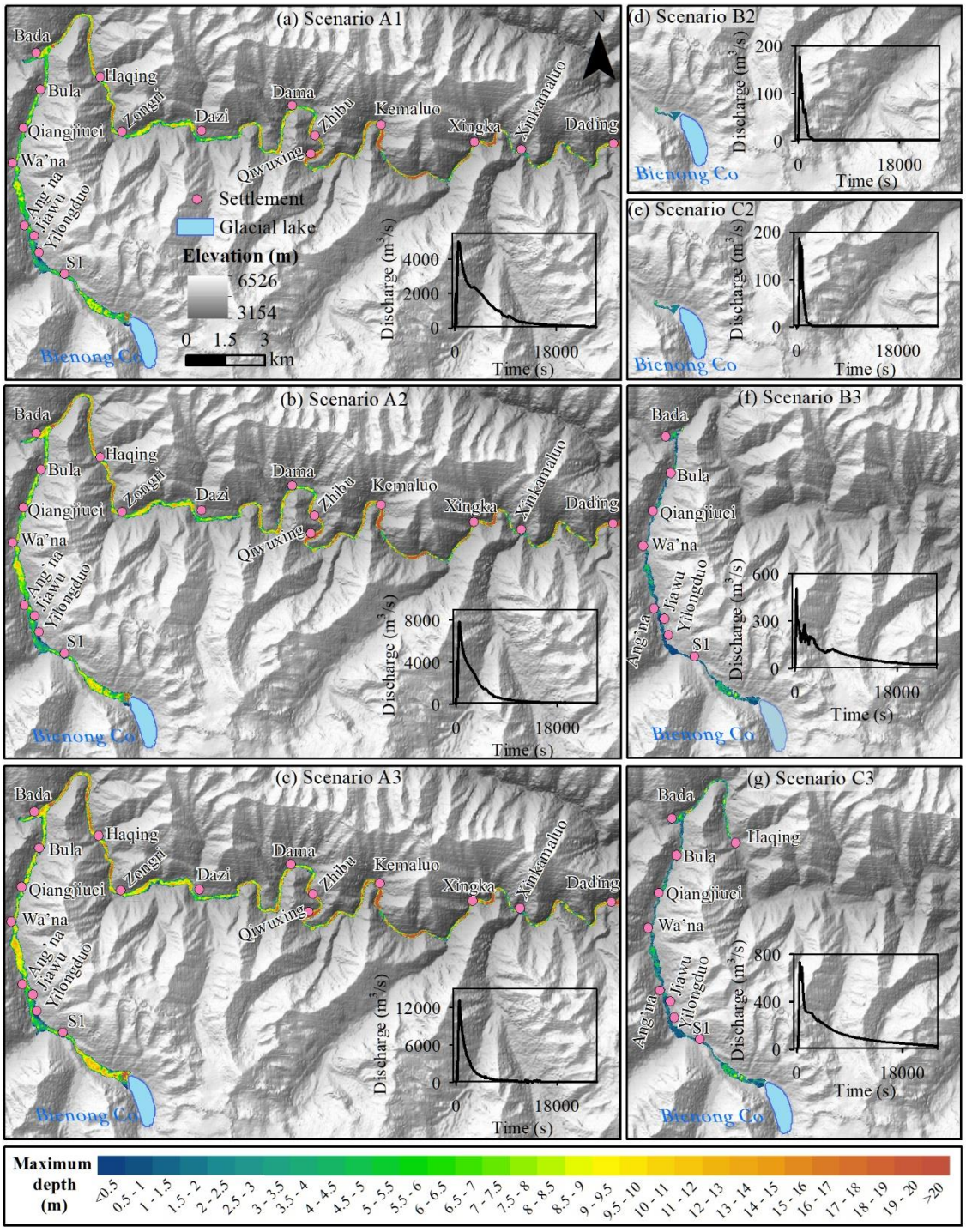

Figure 11. Propagation of flood water downstream and the time series of discharge at the breach outlet (inset) for different scenarios.

GLOFs of different magnitudes pose different potential hazards to each settlement along the flow channel. Scenario A3 produces the most severe threat of GLOF to the downstream region. Six settlements, including Ang'na, Wa'na, Haqing, Kemaluo, Xinka and Dading, will be completely submerged by flooding. Kemaluo village, located 37.9 km downstream of Bienong Co, will experience the relatively largest maximum flow depth of 19.8 m, and the village of Ang'na, having a distance 6.0 km from Bienong Co, will experience the relatively smallest maximum flow depth of 6.1 m. Wa'na village is the most affected of all the villages by GLOF due to the most flooded houses. Eight settlements of S1, Qiangjiuci, Bula, Bada, Dama, Zhibu, Qiwuxing, Xingka and Xinkamaluo will be partial flooded. The maximum flow depth of 11.0 m in Bada village is the largest, and that of 7.2 m in both Dama and Zhibu villages is the smallest. Four settlements, Yilongduo, Jiawu, Zongri and Dazi are spared from flood, in which, Yilongduo may be slightly affected, while Dazi is the safest village owing to its far

distance from river. Flooding in Scenario A2 has a relatively small impact on downstream villages compared to Scenario A3, showing the reduced extent of inundation and flow depth. Ang'na and Haqing villages have reduced flood ranges. However, villages Wa'na, Kemaluo, Xinka and Dading will still be completely flooded, but the maximum flow depth is reduced from 16.5 m, 19.8 m, 12.5 m and 17.5 m to 13.6 m, 19.3 m, 12.0 m and 16.6 m, respectively. For the nine villages partially affected by Scenario A3, they are still affected by flooding of Scenario A2 except for Dama village, but the impact of flooding has a weaken. Scenario A1 differs from Scenario A3 in that Dama and Xingkamaluo villages have been able to be spared from flooding, while other villages have experienced significant reductions in flood extent and inundation depth. The floods of Scenarios B3 and C3 have significantly less impact in the downstream than the above three scenarios. Only Wa'na, Qiangjiuci and Bula villages will be partially affected, with the maximum flow depth of 3.1 m, 1.9 m and 2.0 m in Scenarios B3 and 4.0 m, 2.4 m and 2.7 m in Scenarios C3 (Fig. 12).

The peak discharge and velocity of GLOFs at these villages undergo a gradually decreasing process, while the arrival time of peak discharges is prolonged, favoring the evacuation of residents in the downstream area. Peak discharges in S1, Yilongduo, Jiawu and Ang'na villages are similar for each scenario, ~4,000 m^3/s of Scenario A1, ~6,000 m^3/s of Scenario A2 and ~10,000 m^3/s of Scenario A3. Wa'na, Qiangjiuci, and Bula villages have the similar peak discharges, which are ~3,800 m^3/s, ~5,000 m^3/s, and ~8,000 m^3/s for Scenarios A1, A2, and A3. Since Bula village, peak discharges of each scenario decrease significantly towards the downstream. Taking Scenario A3 as an example, at Bula village, peak discharge is 7,512 m^3/s, to Haqing village, it become smaller than 6,000 m^3/s, to Dama village, it drops below 4,000 m^3/s, to Qiwuxing village drops below 3,000 m^3/s, and at Xinka village decreases to below 1,000 m^3/s (Fig. 13). The flood flow velocity varies dramatically, with Scenarios A1, A2, and A3 corresponding to maximum velocities of 8.9 m/s, 12.2 m/s, and 14.9 m/s, respectively, at village S1. To Dading village, the maximum flow velocity of GLOFs is about 2 m/s.

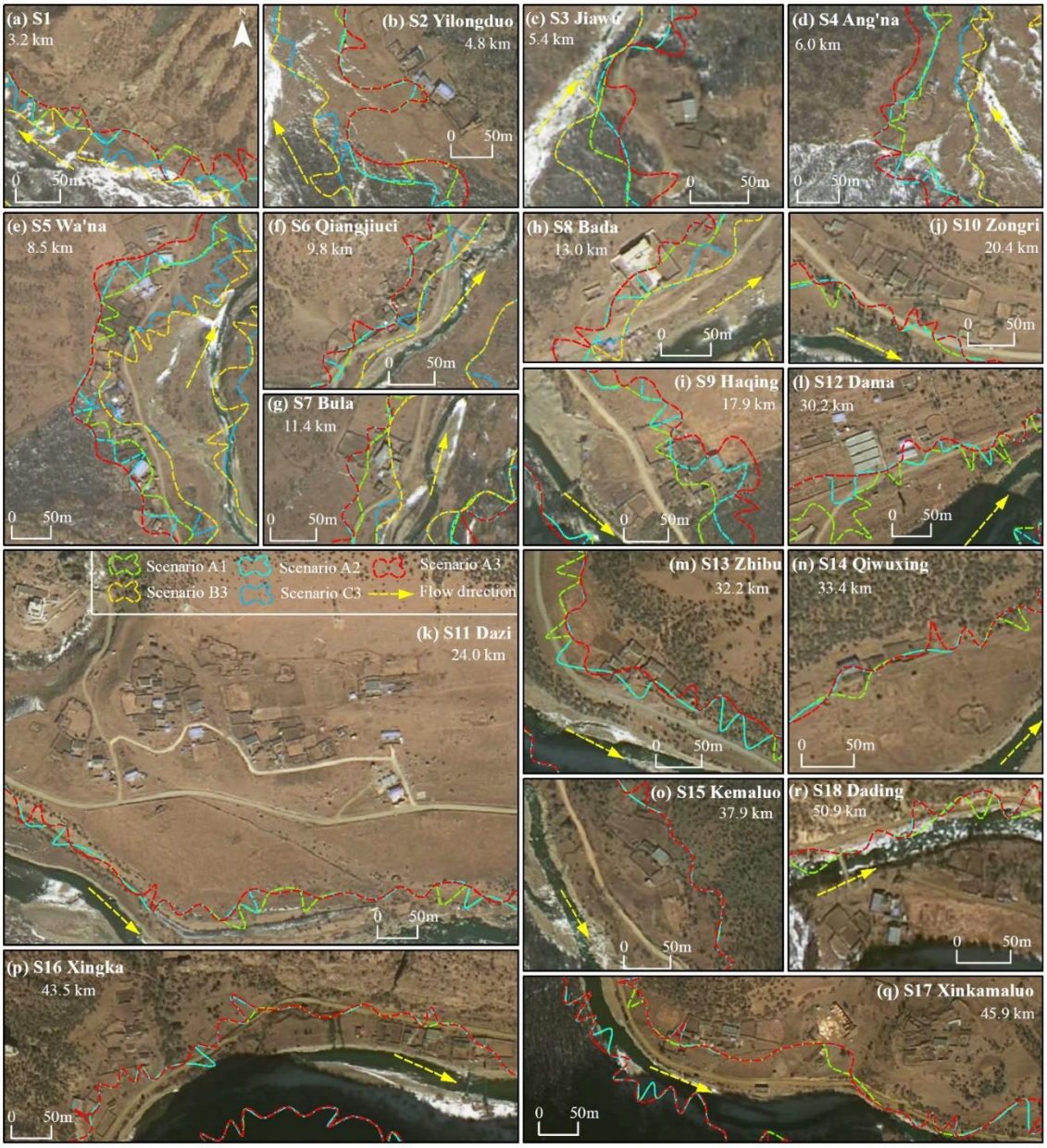

Figure 12. The potential threat of GLOFs to settlements and roads in the downstream under different ice avalanches and landslide scenarios (the background is MapWorld image).

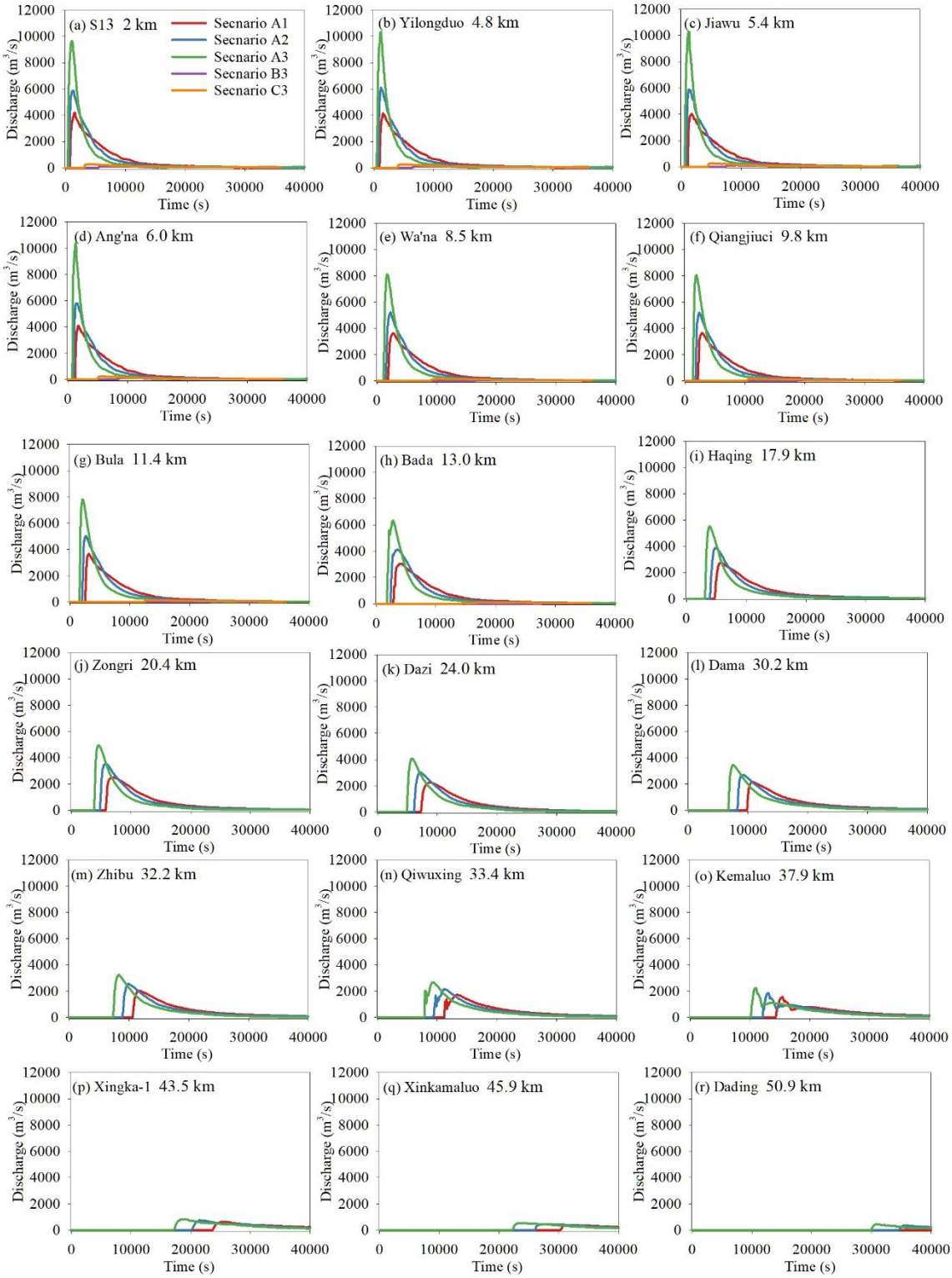

Figure 13. Time series of discharge at different settlements along the flow channel (locations in Fig. 1) of different scenarios.

475

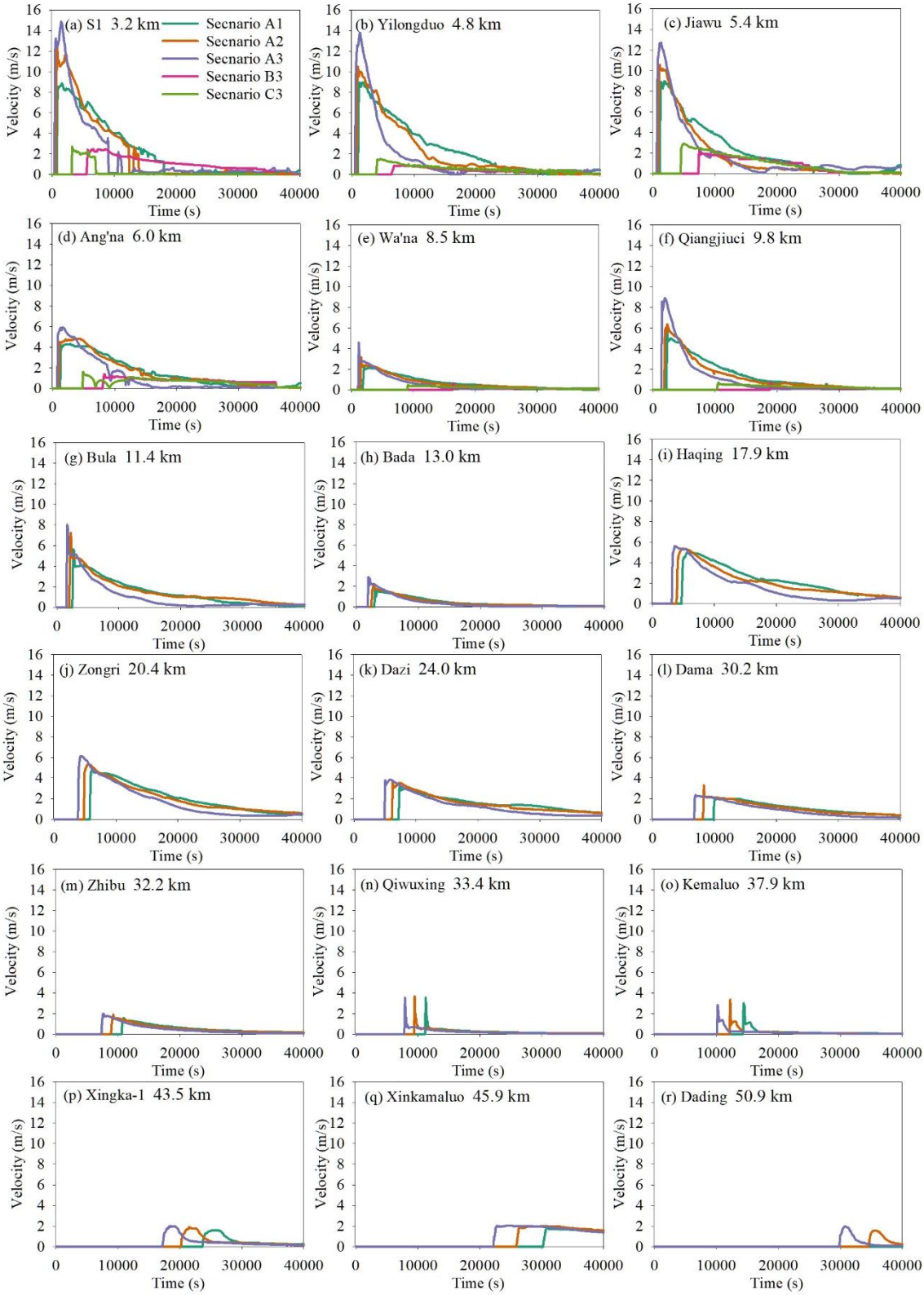

Figure 14. Time series of velocity at different settlements along the flow channel (locations in Fig.1) of different scenarios.

5 Discussion

5.1 Water storage of Bienong Co

Based on the accurate bathymetric results of USV, we obtained that the maximum and depth average of Bienong Co were 181 m and 85.4 m with the water storage of 102.3 × 10^6 m^3 in August 2020. Considering the rarity of bathymetric data but the frequent occurrence of GLOFs in the region, we try to explore more information about glacial lakes in the region by using bathymetry and water storage of Bienong Co. First, relationships with significant correlations for area-volume, area-depth and depth-volume of Bienong Co were established (Fig. 15), and the valuable information is pinned on the hope that could provide a data reference for future studies of Bienong Co and other glacial lakes in the region. Then, we compared the depth and water storage information of Bienong Co with other glacial lakes that have been measured. At present, there are few glacial lakes with measured bathymetry on the Tibetan Plateau, and they are mainly concentrated in the Himalaya of Nepal and the Poiqu basin of Tibet, China. Longbasaba is an end moraine-dammed glacial lake located at the northern slope of the Himalaya, which has an area of 1.22 ± 0.02 km^2 in 2009, with average and maximum depths of 48 ± 2 m and 102 ± 2 m, respectively, storing a water volume of 64 × 10^6 m^3 (Yao et al., 2012). Although the area of Longbasaba is about 6% larger than that of Bienong Co, the water storage is only 60% of that of Bienong Co. This is an example showing that a glacial lake in the maritime glaciation zone is significantly larger in volume than a similarly sized glacial lake in the continental glaciation zone. However, due to the lack of measured bathymetric data of glacial lakes in the continental glaciation zone, no more comparisons can be made. We compared the depth and water storage of Bienong Co with other glacial lakes in the maritime glaciation zone. Comparison between and can be achieved. The area of Lugge glacial lake in Butan was about 1.17 km^2 in 2004, which is slightly larger than that of Bienong Co, but its average depth and maximum depth were 49.8 m and 126 m with water storage of 58 × 10^6 m^3 (Yamada, 2004), which was smaller than the corresponding value of Bienong Co. At the time of bathymetry, both South Lhonak lake in India and Imja glacial lake in Nepal had an area of about 1.3 km^2, which is about 13% larger than that of Bienong Co, but both lakes have 64% and 76% of Bienong Co's water storage, respectively (Sharma et al., 2018; Haritashya et al., 2018). Areas of Raphsthren glacial lake in Buhtan and Tsho Rolpa in Nepal glacial lake were 1.4 km^2 and 1.5 km^2 when bathymetries were carried out, which are 22% and 30% larger than that of Bienong Co, but their water storage are 65% and 84% of that of Bienong Co (Geological survey of India, 1995; ICIMOD, 2011). The area of Lower Barun glacial lake in Nepal was 1.8 km^2, 57% larger than that of Bienong Co, but the water storage was 112 × 10^6 m^3, only 9% larger than that of Bienong Co (Haritashya et al., 2018), showing that Bienong Co is relatively deeper and has a larger storage. This shows that the moraine glacial lakes on the south slope of the Himalayas is very different from that in SETP.

Additionally, due to the scarcity of glacial lake bathymetry data and its importance for GLOF hazard, scholars proposed relationships to estimate volumes of glacial lake through area, width and length (O'Connor et al., 2001; Huggel et al., 2002; Sakai, 2012; Wang et al., 2012a; Yao er al., 2012, Cook and Quincey, 2015; Qi et al., 2022). We estimate the water storage of Bienong Co using published equations based on glacial lakes on the Tibetan Plateau, and the results show that the eight published volume-area/width-length relationships all underestimate the volume of Bienong Co to varying degrees. It can be inferred that Bienong Co is the relative deepest glacial lake among these on the Tibetan Plateau that currently have been measured. Whether this is unique to Bienong Co or a common feature of glacial lakes in the region is not yet known, as few glacial lakes in the region has field bathymetry. Future bathymetry is necessary for more typical glacial lakes in the region.

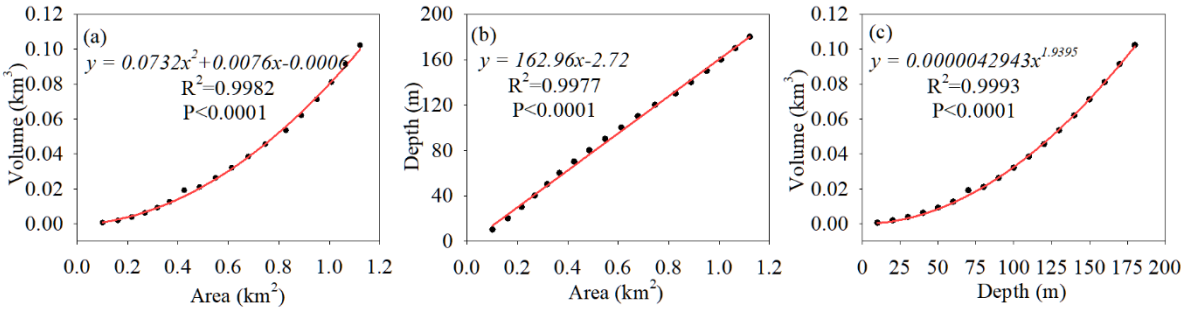

Figure 15. Fitting relationship of (a) area and volume, (b) area and depth and (c) depth and volume of Bienong Co.

Table 1 Calculated volumes of Bienong Co based on published volume-area relationships for glacial lake in Tibetan Plateau.

No	Source		Relationships	Calculated Volume	Error (%)
1	Qi et al., 2022	(1)	$V=0.04066A^{1.184}-0.003207w_{mx}/l_{mx}$	46.9×10^6 m^3	-54%
2		(2)	$V=0.0126A^2+0.0056A+0.0132$	36.3×10^6 m^3	-65%
3	Wang et al., 2012		$V=0.0354A^{1.3724}$	42.9×10^6 m^3	-58%
4	Sakai, 2012		$V=0.04324A^{1.5307}$	53.6×10^6 m^3	-48%
5	Yao et al., 2012		$V=0.0493A^{0.9304}$	56.1×10^6 m^3	-45%
6	Fujita et al., 2013		$V = 0.055A^{1.25}$	65.5×10^6 m^3	-36%
7	Khanal et al., 2015		$V = 0.0578A^{1.5}$	71.3×10^6 m^3	-30%
8	Zhou et al., 2020		$V=0.0717\ w_{mx}^2 l_{mx}$	70.3×10^6 m^3	-31%

Note: Error = (Volume of empirical formulas − Bathymetrically derived volume) / Bathymetrically derived volume × 100%.

5.2 Limitation and uncertainties

Trigger is the beginning of the simulated GLOFs process chain in this study and we only consider ice avalanche and landslide scenarios, instead of other factors, such as increased glacial meltwater and heavy precipitation. The magnitude, location and probability of ice avalanche and landslide are the largest sources of uncertainty in this study. Ice avalanche is the trigger for over 70% of GLOFs on the Tibetan Plateau, but there is no reliable reference to the magnitude including release area and depth of previous ice avalanche events. Ice avalanche in this study come from the mother glacier tongue where the slope is relative steep and fissures are well-developed. We simulated three different-magnitude ice avalanches, each scenario assumes that the ice body breaks off in the vertical direction until to the lake surface, which is unrealistic and may overestimate the volume of ice avalanche. The RAMMS model can estimate the possible release volume based on the input DEM data and the release area as well as the release depth, which are 5×10^6 m^3, 13.1×10^6 m^3 and 41.3×10^6 m^3 for Scenarios A1, A2 and A3. However, simulations show that about 76%, 37% and 14% of the estimated release volume enter the lake in Scenarios A1, A2 and A3, respectively. The simulation duration is set to 600 s to ensure the integrity of the ice avalanche process, however, most of the ice avalanche is already into the lake within 100 s at the beginning. The difference between the volume of the ice avalanche entering the lake and the estimated release volume is mainly influenced by the slope between the ice body and the lake and the distance from the lake. The gentler slope and far distance from the lake of ice body in Scenarios A2 and A3 result in fewer ice avalanches entering the glacial lake, and affect the process of ice avalanche material entering the lake, e.g., Scenarios A2 and A3 have stronger fluctuations in the ice avalanche process than Scenario A1. In addition, we also consider landslide as a trigger given the failure of Jinwu Co in 2020. Two release areas were selected by referring the slope and location of Jinwu Co's landslide. However, the release depth has no quantified reference data and we assumed three release depths of 2 m, 5 m and 10 m for each release area to simulate the consequences resulting from as many scenarios as possible.

Secondly, the grain size distribution of moraine dam of Bienong Co was not obtained in this study, and the simulation

was performed by referencing an inventory of glacial lakes in the Indian Himalaya. Although the data used have been validated to be reliably general, the grain size distribution of the moraine dam of Bienong Co itself would be more useful for an accurate simulation of moraine dam's erosion.

Finally, DEM data are the most important basic data affecting the downstream propagation of GLOFs in this study. ALOS PALSAR DEM data with a spatial resolution of 12.5 m have been widely used in studies related to cryospheric changes and disasters. In this study, the DEM was pre-processed to fill sinks, but there was still the phenomenon of flood water being piled up in some deep puddle during the simulation, i.e., there were errors in the DEM data, especially in the relatively narrow valley. We have manually smoothed several large bumps according to the elevation of the upstream and downstream. However, there are still some smaller bumps that converge the flow to a section of the flow channel, mainly in the downstream area. Therefore, the flooding situation in Qiwuxing, Kemaluo, Xingka and Dading villages might be overestimated, especially in the first two villages because they are relatively far away from the river, while the latter two villages are still very likely to be threatened by flooding due to a close distance to the river. More accurate flood hazard simulations in the future relay on more precise topographic information, such as DEM data generated using panchromatic stereo images with resolutions better than 0.8 m carried by the Gaofen-7 satellite.

6 Conclusion

(1) As a moraine-dammed glacial lake located in the maritime glaciation region, Bienong Co has been highly regarded by local government due to its larger area and high potential of GLOF hazard. Based on bathymetric data, remote sensing images and DEM data, combined with multiple models of RAMMS, BASEMENT and Heller-Hager, we completed a comprehensive investigation of the potential GLOF process chain of Bienong Co, including the initial mass movement from mother glacier and lateral moraine slope, displacement wave generation and propagation in the lake, overtopping flow and erosion on moraine dam and subsequent downstream flooding. The following main conclusions were drawn: According to the field bathymetric data, the lake basin morphology of Bienong Co features a relatively flat basin bottom and the steep flanks, with the slope near the glacier (16.5˚) is steeper than that near the moraine dam (11.3˚). The water storage of Bienong Co was ~102.3×10^6 m^3 in August 2020, with the maximum depth was ~181 m. The huge water storage combined with the fissure-developed mother glacier tongue, steep lateral moraine slope, steep distal facing slope of moraine dam and low freeboard make it of high GLOF potential.

(2) The volume of materials entering the lake for the three scenarios of ice avalanches (A1, A2 and A3) is much larger than the six scenarios of landslides (B1, B2, B3 and C1, C2, C3). Volumes of ice avalanches entering the lake in Scenarios A1, A2 and A3 are 3.8×10^6 m^3, 4.9×10^6 m^3 and 5.8×10^6 m^3, respectively. Among the six landslide scenarios, Scenario B1 releases a minimum volume of 0.03×10^6 m^3 and Scenario C3 releases a maximum volume of 0.30×10^6 m^3. As a result, the impact zone, maximum flow height and maximum flow velocity in the lake also present that Scenarios A1, A2 and A3 are significantly larger than the other six scenarios where Scenario B1 is the smallest and Scenario A3 is the largest. Wave amplitudes near the moraine dam in Scenarios A1, A2, and A3 are 17.1 m, 20.2 m, and 25.2 m, respectively. The overtopping flow of all three scenarios causes erosion of the dam, with little difference in breach depth (19.0 m, 19.1 m and 19.3 m) but large difference in breach width (295.0 m, 339.4 m, and 368.5 m). The volumes of water lost in the lake of the three scenarios are 24.1×10^6 m^3, 25.3×10^6 m^3 and 26.4×10^6 m^3, and the flood peak flows are 4,996 m^3/s, 7,817 m^3/s and 13,078 m^3/s, respectively. Among the other six scenarios, only Scenarios B3 and C3 with larger magnitudes formed breaches on moraine dam, with breaches of 6.5 m and 7.9 m in depth and 153 m and 169 m in width, respectively.

(3) Floods all pass through 18 settlements in the downstream river in 20 hours, with the inundation areas of 7.6 km^2, 8.0 km^2 and 8.5 km^2 as well as average water depths of 8.4 m, 9.1 m and 10.0 m, respectively. The GLOFs threatened more than half of the villages in the downstream region. Scenarios B1/2 and C1/2 produce very limited overtopping flow that cannot pose a threat to the downstream region. Both Scenarios B3 and C3 produced floods that flow through eight downstream

settlements within 20 hours and had a relatively small impact on them.

(4) Bienong Co is the relative deepest glacial lake among these on the Tibetan Plateau that currently have been measured and is very different from glacial lakes on the south slope of the Himalayas. In addition, it is also important to use high-precision topographic data for disaster simulation of glacial lake outburst flood lakes.

Author contributions. HD contributed the conceptualization, methodology, software, formal analysis, visualization and writing of the original draft; XY contributed the conceptualization, supervision, funding acquisition, investigation of the glacial lake, as well as review and editing of the manuscript; YZ, HJ, and QW contributed the investigation of the glacial lake; ZD, BW and QW contributed the model progress; JH contributed the setting up the experimental equipment and obtaining data.

Competing interests. The authors declare that they have no conflict of interest.

Financial support. This research has been supported by the National Key Research Program of China (no. 2019YFE0127700), National Natural Science Foundation of China (grant nos. 41861013 and 42071089), "Innovation Star" of Outstanding Graduate Student Program in Gansu Province (no. 2021-CXZX-215) and Northwest Normal University's 2020 Graduate Research Grant Program (no. 2020KYZZ001012).

References

Aggarwal, A., Jain, S.K., Lohani, A.K., and Jain, N.: Glacial lake outburst flood risk assessment using combined approaches of remote sensing, GIS and dam break modelling. Geom. Nat. Hazard. Risk., 7, 18–36, https://doi.org/10.1080/19475705.2013.862573, 2013.

Allen, S., Rastner, P., Arora, M., Huggel, C., and Stoffel, M.: Lake outburst and debris flow disaster at Kedarnath, June 2013: hydrometeorological triggering and topographic predisposition, Landslides, 13, 1–13, https://doi.org/10.1007/s10346-015-0584-3, 2015.

Byers, A. C., Rounce, D. R., Shugar, D. H. A rockfall-induced glacial lake outburst flood, Upper Barun Valley, Nepal, Landslides, 533-549, https://doi.org/10.1007/s10346-018-1079-916, 2018.

Byers, A. C., Chand, M. B., Lala, J. Reconstructing the History of Glacial Lake Outburst Floods (GLOF) in the Kanchenjunga Conservation Area, East Nepal: An Interdisciplinary Approach, Sustainability, 12, 5407, https://doi.org/10.3390/su12135407, 2020.

Brunner, G.W.: HEC-RAS River Analysis System: User's Manual. US Army Corps of Engineers. Institute for Water Resources, Hydrologic Engineering Center, 2002.

Brun, F., Berthier, E., Wagnon, P., Kääb, A., and Treichler, D.: A spatially resolved estimate of High Mountain Asia glacier mass balances from 2000 to 2016, Nat. Geosci., 10, 668–673, https://doi.org/10.1038/ngeo2999, 2017.

Carrivick, J. L. and Tweed, F. S.: A global assessment of the societal impacts of glacier outburst floods, Global. Planet. Change., 144, 1–16, https://doi.org/10.1016/j.gloplacha.2016.07.001, 2016.

Cheng, Z., Zhu, P., Dang, C., and Liu, J.: Hazards of debris flow due to glacier lake outburst in Southeastern Tibet, Journal of Glaciology and Geocryology, 30, 954–959, https://doi.org/CNKI:SUN:BCDT.0.2008-06-006, 2008.

Cheng, Z. L., Liu, J. J., and Liu, J. K.: Debris flow induced by glacial-lake break in Southeast Tibet, Earth Science Frontiers, 16, 207–214, https://doi.org/10.2495/DEB100091, 2009.

Christen, M., Kowalski, J., Bartelt, P., RAMMS: numerical simulation of dense snow avalanches in three-dimensional terrain. Cold Reg. Sci. Technol. 63, 1–14, 2010.

Clague, J. J. and Evans, S. G.: A review of catastrophic drainage of moraine-dammed lakes in British Columbia, Quaternary. Sci. Rev., 19, 1763–1783, https://doi.org/10.1016/S0277-3791(00)00090-1, 2000.

Cook, S. J. and Quincey, D. J.: Estimating the volume of Alpine glacial lakes. Earth. Surf. Dynam., 3, 559–575, https://doi.org/10.5194/esurf-3-559-2015, 2015.

Cook, K. L., Andermann, C., Gimbert, F., Adhikari, B. R., and Hovius, N.: Glacial lake outburst floods as drivers of fluvial erosion in the Himalaya, Science, 362, 53–57, https://doi.org/10.1126/ science.aat 4981, 2018.

Coon, W. F.: Estimation of roughness coefficients for natural stream channels with vegetated banks, United States Geological Survey water-supply paper, 2441, 1998.

Cui, P., Ma, D. T., and Chen, N. S.: The initiation, motion and mitigation of debris flow caused by glacial lake outburst, Quaternary Sciences, 23, 621–628, https://doi.org/10.1016/S0955-2219(02)00073-0, 2003.

Dehecq, A., Gourmelen, N., Gardner, A. S., Brun, F., Goldberg, D., Nienow, P. W., Berthier, E., Vincent, C., Wagnon, P., and Trouvé, E.: Twenty-first century glacier slowdown driven by mass loss in High Mountain Asia, Nat. Geosci., 12, 22–27, https://doi.org/10.1038/s41561-018-0271-9, 2019.

Duan, H. Y., Yao, X. J., Zhang, D. H., Qi, M. M., and Liu, J.: Glacial Lake Changes and Identification of Potentially Dangerous Glacial Lakes in the Yi'ong Zangbo River Basin, Water-Sui, 12, 538, https://doi.org/10.3390/w12020538, 2020.

Dwivedi, S. K., Acharya, M., and Simard, R.: The Tam Pokhari Glacier Lake outburst flood of 3 September 1998, Journal of Nepal Geological Society, 22, 539–546, https://doi.org/10.3126/jngs.v22i0.32429, 2000.

Emmer, A. and Cochachin, A.: The causes and mechanisms of moraine-dammed lake failures in the Cordillera Blanca, North American Cordillera and Himalaya, AUC. Geogr., 48, 5–15, https://doi.org/10.14712/23361980.2014.23, 2013.

Emmer, A. and Vilímek, V. New method for assessing the susceptibility of glacial lakes to outburst floods in the Cordillera Blanca, Peru, Hydrol Earth Syst Sc, 18, 3461–3479, https://doi.org/10.5194/hess-18-3461-2014, 2014.

Evans, S. G.: The maximum discharge of outburst floods caused by the breaching of man-made and natural dams, reply. Can. Geotech. J., 24, 385–387, https://doi.org/10.1139/t87-062, 1987.

Fujita, K., Sakai, A., Takenaka, S., Nuimura, T., Surazakov, A. B., Sawagaki, T., and Yamanokuchi, T.: Potential flood volume of Himalayan glacial lakes, Nat. Hazard. Earth. Sys., 13, 1827–1839, https://doi.org/10.5194/nhess-13-1827-2013, 2013.

Geological Survey of India: Geology environmental hazards and remedial measures of the Lunana Area, Gasa Dzongkhang, Report of 1995 Indo-Bhutan Expedition, Bhutan Unit, Geological Survey of India, Samtse, 1995.

Guo, W. Q., Liu, S. Y., Xu, J. L., Wu, L. Z., Shangguan, D. H., Yao, X. J., Wei, J. F., Bao, W. J., Yu, P. C., Liu, Q., and Jiang, Z. L.: The second Chinese glacier inventory: Data, methods and results, J. Glaciol., 61, 357-372, https://doi.org/10.3189/2015JoG14J209, 2015.

Haeberli, W., Kääb, A.,Vonder Mühll, D., Teysseire, P. Prevention of outburst floods from periglacial lakes at Grubengletscher, Valais, Swiss Alps, J. Glaciol. 47, 111–122, 2001

Haritashya, U. K., Kargel, J. S., Shugar, D. H., Leonard, G. J., Strattman, K., Watson, C. S., Shean, D., Harrison, S., Mandli, K. T., and Regmi, D.: Evolution and controls of large glacial lakes in the Nepal Himalaya, Remote Sens-Basel, 10, 798, https://doi.org/10.3390/rs10050798, 2018.

Heller, V., Hager, W., and Minor, H. E. Landslide generated im- pulse waves in reservoirs: Basics and computation. Laboratory Of Hydraulics, Hydrology, and Glaciology, ETH Zürich, Switzerland, 172 pp, 2009.

Huang, L., Zhu, L. P., Wang, J. B., Ju, J. T., Wang, Y., Zhang, J. F., and Yang, R. M.: Glacial activity reflected in a continuous lacustrine record since the early Holocene from the proglacial Laigu Lake on the southeastern Tibetan Plateau, Palaeogeogr, Palaeocl., 456, 37–45, https://doi.org/10.1016/j.palaeo.2016.05.019, 2016.

Huggel, C., Kääb, A., Haeberli, W., Teysseire, P., and Paul, F.: Remote sensing based assessment of hazards from glacier lake outbursts: a case study in the Swiss Alps, Can. Geotech. J., 39, 316–330, https://doi.org/10.1139/t01-099, 2002.

Huggel, C., Haeberli, W., Kääb, A., Bieri, D., and Richardson, S.: An assessment procedure for glacial hazards in the Swiss Alps, Can. Geotech. J., 41, 1068–1083, https://doi.org/10.1139/t04-053, 2004.

International Centre for Integrated Mountain Development (ICIMOD): Glacial Lakes and Glacial Lake Outburst Floods in

Nepal. ICIMOD, Kathmandu, 99, 2011.

Jain, S.K., Lohani, A.K., Singh, R.D., Chaudhary, A., and Thakural, L.N.: Glacial lakes and glacial lakes outburst flood in a Himalayan basin using remote sensing and GIS. Nat. Hazard., 62, 887–899, https://doi.org/10.1007/s11069-012-0120-x, 2012.

Kääb, A., Berthier, E., Nuth, C., Gardelle, J., and Arnaud, Y.: Contrasting patterns of early twenty-first-century glacier mass change in the Himalayas, Nature, 488, 495–498, https://doi.org/10.1038/nature11324, 2012.

Kääb, A., Treichler, D., Nuth, C., and Berthier, E.: Brief communication: contending estimates of 2003-2008 glacier mass balance over the Pamir-Karakoram-Himalaya, The Cryosphere, 9, 557–564, https://doi.org/10.5194/tc-9-557-2015, 2015.

Ke, C. Q., Kou, C., Ludwig, R., and Qin, X.: Glacier velocity measurements in the eastern Yigong Zangbo basin, Tibet, China, J. Glaciol., 59, 1060–1068, https://doi.org/10.3189/2013jog12j234, 2013.

Ke, C. Q., Han, Y. F., and Kou, C.: Glacier Change in the Yigong Zangbu Basin, Tibet, China (1988 to 2010), Dragon 3 Mid Term Results, November 2014, http://articles.adsabs.harvard.edu/pdf/2014ESASP.724E.16K, 2014.

Lala, J. M., Rounce, D. R., and Mckinney, D. C.: Modeling the glacial lake outburst flood process chain in the Nepal Himalaya: Reassessing Imja Tsho's hazard, Hydro. Earth. Syst. Sc., 22, 3721–3737, https://doi.org/10.5194/hess-2017-683, 2018.

Larrazabal, J. M. and Peñas, M. S.: Intelligent rudder control of an unmanned surface vessel, Expert. Syst. Appl., 55, 106–117, https://doi.org/10.1016/j.eswa.2016.01.057, 2016.

Li, J.J., Zhen, B. X., and Yang, X. J.: Glaciers in Tibet. Science Press, Beijing, 1986.

Li, D., Shangguan D. H., Wang, X.Y., Ding, Y. J., Su, P. C., Liu, R. L., and Wang, M. X.: Expansion and hazard risk assessment of glacial lake Jialong Co in the central Himalayas by using an unmanned surface vessel and remote sensing, Sci. Total. Environ., 784, 147249, https://doi.org/10.1016/j.scitotenv.2021.147249, 2021.

LIGG/WECS/NEA: Report on First Expedition to Glaciers and Glacier Lakes in the Pumqu (Arun) and Poiqu (Bhote-Sun Koshi) River Basins, Xizang (Tibet), China. Sino-Nepalese Joint Investigation of Glacier Lake Outburst Flood in Himalayas in 1987, 192, 1988.

Liu, J., Yao, X. J., Gao, Y. P., Qi, M. M., Duan, H. Y., and Zhang, D. H.: Glacial lake variation and hazards assessment of glacial lakes outburst in the Parlung Zangbo River Basin, Journal of Lake Sciences, 31, 1132–1143, https://doi.org/10.18307/2019.0420, 2019.

Liu, J. K., Zhou, L. X., Zhang, J. J., and Zhao, W. Y.: Characteristics of Jiwencuo GLOF, Lhari county, Tibet. Geological Review, 67: 17–18. https://doi.org/10.16509/j.georeview.2021.s1.007, 2021.

Liu S.Y., Pu J. C., and Deng, X. F.: Glaciers and Glacier Landscapes in China. Shanghai Popular Science Press, Shanghai 38–41, 2014.

Liu, W. M., Lai, Z. P., Hu, K. H., Ge, Y. G, Cui, P., Zhang, X. G., and Liu, F.: Age and extent of a giant glacial-dammed lake at Yarlung Tsangpo gorge in the Tibetan Plateau, Geomorphology, 246, 370–376, https://doi.org/10.1016/j.geomorph.2015.06.034, 2015.

Liu, Z. X., Zhang, Y. M., Yu, X., and Yuan, C.: Unmanned surface vehicles: an overview of developments and challenges, Annu. Rev. Control., 41, 71–39, https://doi.org/10.1016/j. arcontrol.2016.04.018, 2016.

Liu, J. k., Zhang, J. J., Gao, Bo., Li, Y. L., Li, M. Y., Wujin, D. J., Zhou, L. X. An overview of glacial lake outburst flood in Tibet, China. Journal of Glaciology and Geocryology, 41, 1335–1347, https://doi.org/10.7522/j.issn.1000-0240.2019.0073, 2019.

Lliboutry, L.: Glaciological problems set by the control of dangerous lakes in Cordillera Blanca, Peru. II. Movement of a covered glacier embedded within a rock glacier, J. Glaciol., 18, 255–274, https://doi.org/10.3189/S0022143000021341, 1977.

Lohani, A.K. and Jain, S.K.: Analysis of Glacier Lake Outburst Floods. Bharatiya Vaigyanik Evam Audyogik Anusandhan Patrika (BVAAP) 24, 55–59, 2016.

Lv, R. R., Tang, X. B., and Li, D. J.: Glacial lake outburst mudslide in Tibet, Chengdu University of Science and Technology Press, Chengdu, 69–105, 1999.

Mckillop, R. J. and Clague, J. Statistical, remote sensing-based approach for estimating the probability of catastrophic drainage from moraine-dammed lakes in southwestern British Columbia, Global Planet Change, 56, 153–171, https://doi.org/10.1016/J.GLOPLACHA.2006.07.004, 2007.

Mergili, M. and Schneider, J. F.: Regional-scale analysis of lake outburst hazards in the southwestern Pamir, Tajikistan, based on remote sensing and GIS, Nat. Hazard. Earth. Sys., 11, 1447–1462, https://doi.org/10.5194/nhess-11-1447-2011, 2011.

Mergili, M., Fischer, J. T., Krenn, J., and Pudasaini, S. P.: r.avaflow v1, an advanced open-source computational framework for the propagation and interaction of two-phase mass flows, Geosci. Model Dev., 10, 553–569, https://doi.org/10.5194/gmd-10-553-2017, 2017.

Mergili, M. and Pudasaini, S. P.: r.avaflow–The open source mass flow simulation model, available at: https://www.avaflow.org/, last access: 30 October 2020.

Mir, R. A., Jain, S. K., Lohani, A. K., and Saraf, A. K.: Glacier recession and glacial lake outburst flood studies in Zanskar basin, western Himalaya, J. Hydrol., 564, 376-396, https://doi.org/10.1016/j.jhydrol.2018.05.031, 2018.

Mool, P.K., Bajracharya, S.R., and Joshi, S.P.: Inventory of Glaciers, Glacial Lakes and Glacial Lake Outburst Floods, Monitoring and Early Warning Systems in the Hindu Kush- Himalayan Region: Nepal, ICIMOD & UNEP RRC-AP, 363, 2001.

Neckel, N., Kropáček, J., Bolch, T., and Hochschild, V.: Glacier mass changes on the Tibetan Plateau 2003–2009 derived from ICESat laser altimetry measurements, Environ. Res. Lett., 9, 468–475, https://doi.org/10.1088/1748-9326/9/1/014009, 2013.

Nie, Y., Liu, Q., Wang, J. D., Zhang, Y. L., Sheng, Y. W., and Liu, S. Y.: An inventory of historical glacial lake outburst floods in the Himalayas based on remote sensing observations and geo-morphological analysis, Geomorphology, 308, 91–106, https://doi.org/10.1016/j. geomorph.2018.02.002, 2018.

O'Connor, J. E., Hardison, J. H., and Costa, J. E.: Debris flows from failures of neoglacial-age moraine dams in the Three Sisters and Mount Jefferson wilderness areas, Oregon, United States Geological Survey Professional Paper, 1606, 11–40, https://doi.org/10.1007/BF01211117, 2001.

Osti, R. and Egashira, S.: Hydrodynamic characteristics of the Tam Pokhari glacial lake outburst flood in the Mt. Everest region, Nepal, Hydrol. Process., 23, 2943–2955, https://doi.org/10.1002/hyp.7405, 2009.

Osti, R., Bhattarai, T. N., and Miyake, K.: Causes of catastrophic failure of Tam Pokhari moraine dam in the Mt. Everest region, Nat. Hazards, 58, 1209–1223, https://doi.org/10.1007/s11069-011-9723-x, 2011.

Prakash, C. and Nagarajan, R.: Outburst susceptibility assessment of moraine-dammed lakes in Western Himalaya using an analytic hierarchy process, Earth. Surf. Proc. Land., 42, 2306–2321, https://doi.org/10.1002/esp.4185, 2017.

Pudasaini, S. P. and Mergili, M.: A Multi-Phase MassFlow Model, J. Geophys. Res.-Earth, 124, 2920–2942, https://doi.org/10.1029/2019jf005204, 2019.

Qi, M. M., Liu, S. Y., Yao, X. J., R, Grünwald., and Liu, J.: Lake inventory and potentially dangerous glacial lakes in the Nyang Qu Basin of China between 1970 and 2016, J. Mt. Sci-Engl, 17, 851–870, https://doi.org/10.1007/s11629-019-5675-5, 2020.

Qin D. H., Dong, W. J., and Luo, Y.: Climate and Environment Change in China. China Meteorologiacal Press, Beijing, 116-121, 2012.

Richardson, S. D. and Reynolds, J. M.: An overview of glacial hazards in the Himalayas, Quatern. Int., 65, 31–47, https://doi.org/10.1016/S1040-6182(99)00035-X, 2000.

Risio, M., Girolamo, P. D., and Beltrami, G. M.: Forecasting landslide generated Tsunamis: a review, the Tsunami threat-research and technology, 81–106, https://doi.org/10.5772/13767, 2011.

Rounce, D. R., McKinney, D. C., Lala, J. M., Byers, A. C., and Watson, C. S.: A new remote hazard and risk assessment framework for glacial lakes in the Nepal Himalaya, Hydrol. Earth. Syst. Sc., 20, 3455–3475, https://doi.org/10.5194/hess-20-3455-2016, 2016.

Sakai, A., Yamada, T., and Fujita, K.: Volume Change of Imja Glacial Lake in the Nepal Himalayas. International Symposium

on Disaster Mitigation & Basin Wide Water Management, Niigata, 2003, 556–561. 2003.

Sakai, A.: Glacial lakes in the Himalayas: a review on formation and expansion processes, Global Environmental Research, 16, 23–30, 2012.

Sattar, A., Goswami, A., and Kulkarni, A. V.: Hydrodynamic moraine-breach modeling and outburst flood routing–a hazard assessment of the South Lhonak lake, Sikkim, Sci. Total. Environ., 668, 362–378, https://doi.org/10.1016/j.scitotenv.2019.02.388, 2019.

Sattar, A., Haritashya, U. K., Kargel, J. S., Leonard, G. J., and Chase, D. V.: Modeling Lake Outburst and Downstream Hazard Assessment of the Lower Barun Glacial Lake, Nepal Himalaya, J. Hydrol., 598, 126208, https://doi.org/10.1016/j.jhydrol.2021.126208, 2021.

Schneider, D., Huggel, C., Cochachin, A., Guillén, S., García, J. Mapping hazards from glacier lake outburst floods based on modelling of process cascades at Lake 513, Carhuaz, Peru. Adv. Geosci, 35, 145–155, https://doi.org/10.5194/adgeo-35-145-2014, 2014.

Sharma, R. K., Pradhan, P., Sharma, N. P., and Shrestha, D. G.: Remote sensing and in situ-based assessment of rapidly growing South Lhonak glacial lake in eastern Himalaya, India, Nat. Hazards., 93, 393, https://doi.org/10.1007/s11069-018-3348-2, 2018.

Shi, W. L., Yang, C. T., You, G. X., and Jin, M. X.: The measurement of reserve of glacier block lake on the upper stream of Yerqiang river and the calculation of its maximum flood, Arid Land Geography., 14, 31–35, 1991.

Song, C., Sheng, Y., Ke, L., Nie, Y., and Wang, J.: Glacial lake evolution in the southeastern Tibetan Plateau and the cause of rapid expansion of proglacial lakes linked to glacial-hydrogeomorphic processes, J. Hydrol., 540, 504–514, https://doi.org/10.1016/j.jhydrol.2016.06.054, 2016.

Somos-Valenzuela, M.A., Chisolm, R.E., Rivas, D.S., Portocarrero, C., McKinney, D.C. Modeling glacial lake outburst flood process chain: the case of Lake Palcacocha and Huaraz, Peru. Hydrol Earth Syst Sc, 20, 2519–2543, https://doi.org/10.5194/hess-2015-512.Specht, M., Specht, C., Lasota, H., and Cywiński, P.: Assessment of the steering precision of a hydrographic unmanned surface vessel (USV) along sounding profiles using a low-cost multi-global navigation satellite system (GNSS) receiver supported autopilot, Sensors-Basel, 19, 3939, https://doi.org/10.3390/s19183939, 2019a.

Sun, M. P., Liu, S. Y., Yao, X. J., and Li, L.: The cause and potential hazard of glacial lake outburst flood occurred on July 5, 2013 in Jiali County, Tibet, Journal of Glaciology and Geocryology, 36, 158–165, https://doi.org/158-165,10.7522/j.issn.1000-0240.2014.0020, 2014.

Thakur, P.K., Aggarwal, S., Aggarwal, S.P., and Jain, S.K.: One-dimensional hydro-dynamic modeling of GLOF and impact on hydropower projects in Dhauliganga Riverusing remote sensing and GIS applications. Nat. Hazard., 83, 1057–1075, https://doi.org/10.1007/s11069-016-2363-4, 2016.

Thompson, S., Benn, D. I., Mertes, J., and Luckman, A.: Stagnation and mass loss on a himalayan debris-covered glacier: Processes, patterns and rates, J. Glaciol., 62, 467–485, https://doi.org/10.1017/jog.2016.37, 2016.

Veh, G., Korup, O., Specht, S. V., Roessner, S., and Walz, A.: Unchanged frequency of moraine-dammed glacial lake outburst floods in the Himalaya, Nat. Clim. Change., 9, 379–383, https://doi.org/10.1038/s41558-019-0437-5, 2019.

Vetsch, D., Siviglia, A., Ehrbar, D., Facchini, M., Kammerer, S., Koch, A., Peter, S., Vonwiller, L., Gerber, M., Volz, C., Farshi, D., Mueller, R., Rousselot, P., Veprek, R., and Faeh, R.: System Manuals ofBASEMENT, Version 2.7. Laboratory of Hydraulics, Glaciology and Hydrology (VAW), ETH Zurich, available at: http://www.basement.ethz.ch, last access: 3 October 2022.

Vilímek, V., Emmer, A., Huggel, C., Schaub, Y., and Würmli, S.: Database of glacial lake outburst floods (GLOFs)–IPL project no. 179, Landslides, 11, 161–165, https://doi.org/10.1007/s10346-013-0448-7, 2013.

Wang, S. J., Yang, Y., Gong, W., Che, Y., Ma, X., and Xie, J.: Reason analysis of the Jiwenco glacial lake outburst flood (GLOF) and potential hazard on the Qinghai-Tibetan Plateau, Remote Sens-Basel, 13, 3114, https://doi.org/10.3390/rs13163114, 2021.

Wang, W. C., Yao, T. D., Gao, Y., Yang, X. X., and Kattel, D. B.: A first-order method to identify potentially dangerous glacial

lakes in a region of the southeastern Tibetan Plateau, Mt. Res. Dev., 31, 122–130, https://doi.org/10.1659/MRD-JOURNAL-D-10-00059.1, 2011a.

Wang, W. C., Yang, X. X., and Yao, T. D.: Evaluation of ASTER GDEM and SRTM and their suitability in hydraulic modelling of a glacial lake outburst flood in southeast Tibet, Hydrol. Process., 26, 213–225, https://doi.org/10.1002/hyp.8127, 2011b.

Wang, W. C., Yao, T. D., Yang, W., Joswiak, D., and Zhu, M. L.: Methods for assessing regional glacial lake variation and hazard in the southeastern Tibetan Plateau: a case study from the Boshula mountain range, China, Environ. Earth. Sci., 67, 1441–1450, https://doi.org/ 10.1007/s12665-012-1589-z, 2012.

Wang, W. C., Gao, Y., Anacona, P. I., Lei, Y. B., Xiang, Y., Zhang G. Q., Li, S. H., and Lu, A. X.: Integrated hazard assessment of Cirenmaco glacial lake in Zhangzangbo valley, Central Himalayas, Geomorphology, 306, 292–305, https://doi.org/10.1016/j.geomorph.2015.08.013, 2015.

Wang, X., Liu, S. Y., Ding, Y. J., Guo, W. Q., Jiang, Z. L., Lin, J., and Han, Y.: An approach for estimating the breach probabilities of moraine-dammed lakes in the chinese himalayas using remote-sensing data. Nat. Hazard. Earth. Sys., , 12, 3109-3122, https://doi.org/10.5194/nhess-12-3109-2012, 2012a.

Wang, X., Liu, S. Y., Guo, W. Q., Yao, X. J., Jiang, Z. L., and Han, Y. S: Using Remote Sensing Data to Quantify Changes in Glacial Lakes in the Chinese Himalaya, Mt. Res. Dev., 32, 203–212, https://doi.org/10.1659/MRD-JOURNAL-D-11-00044.1, 2012b.

Wang X. Methodology and application of moraine lake outburst hazard evaluation in the Chinese Himalayas, Science Press, Beijing, 2016.

Wang, X., Chai, K. G., Liu, S. Y., Wei, J. F., Jiang, Z. L., and Liu, Q. H.: Changes of glaciers and glacial lakes implying corridor-barrier effects and climate change in the Hengduan Shan, southeastern Tibetan Plateau, J. Glaciology., 63, 535–542, https://doi.org/10.1017/jog.2017.14, 2017.

Watanbe, T. and Rothacher, D.: The 1994 Lugge Tsho glacial lake outburst flood, Bhutan Himalaya, Mt. Res. Dev., 16, 77–81, h https://doi.org/10.2307/3673897, 1996.

Watson, C. S., Quincey, D. J., Carrivick, J. L., Smith, M. W., Rowan, A. V., and Richardson, R.: Heterogeneous water storage and thermal regime of supraglacial ponds on debris covered glaciers, Earth. Surf. Proc. Land., 43, 229–241, https://doi.org/10.1002/esp.4236, 2018.

Westoby, M. J., Glasser, N. F., Brasington, J., Hambrey, M. J., Quincey, D. J., and Reynolds, J. M.: Modelling outburst floods from moraine-dammed glacial lakes, Earth-Sci. Rev., 134, 137–159, https://doi.org/10.1016/j.earscirev.2014.03.0092014, 2014.

Worni, R., Stoffel, M., Huggel, C., Volz, C., Casteller, A., and Luckman, B.: Analysis and dynamic modeling of a moraine failure and glacier lake outburst flood at Ventisquero Negro, Patagonian Andes (Argentina), J. Hydrol., 444–445, 134–145, https://doi.org/10.1016/j.jhydrol.2012.04.013, 2012.

Worni, R., Huggel, C., Clague, J. J., Schaub, Y., and Stoffel, M.: Coupling glacial lake impact, dam breach, and flood processes: A modeling perspective, Geomorphology, 224, 161–176, https://doi.org/10.1016/j.geomorph.2014.06.031, 2014.

Wong, M. and Parker, G. Reanalysis and correction of bed-load relation of meyer-peter and mã¼ller using their own database. Journal of Hydraulic Engineering, 132, 1159–1168, https://doi.org/10.1111/j.1600-0587.1978.tb00950.x, 2006.

Xie, Z. C., and Liu, C. H: Introduction to Glaciology. Shanghai Science Popular Press, Shanghai, 425–426, 2010.

Yan, R. J., Pang, S., Sun, H. B., and Pang, Y. J.: Development and missions of unmanned surface vehicle, J. Mar. Sci. Appl., 9(4), 451–457, https://doi.org/10.1007/s11804-010-1033-2, 2010.

Yang, W., Yao, T. D., Xu, B. Q., Wu, G. J., Ma, L. L., and Xin, X. D.: Quick ice mass loss and abrupt retreat of the maritime glaciers in the Kangri Karpo Mountains, southeast Tibetan Plateau, Chin. Sci. Bull., 53, 2547–2551, https://doi.org/10.1007/s11434-008-0288-3, 2008.

Yamada, T.: Glacier lake and its outburst flood in the Nepal Himalaya. Data Center for Glacier Research, Japanese Society of

Snow and Ice, 1, 96, 1998.

Yamada, T. N., Naito, S., Kohshima, H., Fushimi, F., Nakazawa, T., Segawa, J., Uetake, R., Suzuki, N., Sato, Karma, I. K., Chhetri, L., Gyenden, H., Yabuki, and Chikita, K.: Outline of 2002: research activity on glaciers and glacier lakes in Lunana region, Bhutan Himalayas. Bull. Glaciol. Res., 21: 79–90, 2004.

Yao, X. J., Liu, S. Y., Sun, M. P., Wei, J. F., and Guo, W. Q.: Volume calculation and analysis of the changes in moraine-dammed lakes in the north Himalaya: a case study of Longbasaba lake, J. Glaciol, 58, 753–760, https://doi.org/10.3189/2012JoG11J048, 2012.

Yao, X. J., Liu, S. Y., Sun, M. P., and Zhang, X. J.: Study on the Glacial Lake Outburst Flood Events in Tibet since the 20th Century, Journal of Natural Resources, 8, 1377–1390, https://doi.org/10.11849/zrzyxb.2014.08.010, 2014.

Yuan, G. and Zeng, Q.: Glacier-dammed Lake in Southeastern Tibetan Plateau during the Last Glacial Maximum, J. Geol. Soc. India., 79, 295–301, https://doi.org/10.1007/s12594-012-0041-z, 2012.

Zemp, M., Huss, M., Thibert, E., Eckert, N., McNabb, R., Huber, J., Barandun, M., Machguth, H., Nussbaumer, S. U., Gartner-Roer, I., Thomson, L., Paul, F., Maussion, F., Kutuzov, S., and Cogley, J. G.: Global glacier mass changes and their contributions to sea-level rise from 1961 to 2016, Nature, 568, 382–386, https://doi.org/10.1038/s41586-019-1071-0, 2019.

Zhang, B., Liu, G. X., Zhang, R., Fu, Y., and Li, Z. L.: Monitoring dynamic evolution of the glacial lakes by using time series of Sentinel-1A SAR images, Remote Sens-Basel, 13, 1313, https://doi.org/10.3390/rs13071313, 2021.

Zhang, M. M., Chen, F., Tian, B. S., Liang, D., and Yang, A. Q.: High-frequency glacial lake mapping using time series of Sentinel-1A/1B SAR imagery: An assessment for southeastern Tibetan Plateau, Nat. Hazard. Earth. Sys., 1–18, https://doi.org/10.5194/nhess-2019-219, 2020.

Zhang, Y., Yao, X. J., Duan, H. Y., and Wang, Q.: Simulation of Glacial Lake Outburst Flood in Southeastern Qinghai-Tibet Plateau—A Case Study of JiwenCo Glacial Lake, Fronter in Earth Science, Frontiers in Earth Science, 10: 1–13. https://doi: 10.3389/feart.2022.819526, 2022.

Zheng, G. X., Mergili, M., Emmer, A., Allen, S., and Stoffel, M.: The 2020 glacial lake outburst flood at Jinwuco, Tibet: causes, impacts, and implications for hazard and risk assessment, The Cryosphere, 15, 3159–3180, https://doi.org/10.5194/tc-2020-379, 2021.

Zhou, L. X., Liu, J. K., Li, Y. L.: Calculation method of mathematical model of the moraine dammed lake storage capacity. Science Technology and Engineering, 2020, 20: 9804–9809.